Journal Pre-proof

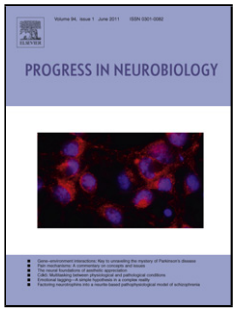

PLA2 G4E, a candidate gene for resilience in Alzheimerś disease and a new target for dementia treatment

Marta Perez-Gonzalez, Maite Mendioroz, Sara Badesso, Diego Sucunza, Miren Roldan, Maria Espelosín, Susana Ursua, Rafael Lujan, Mar Cuadrado-Tejedor, Ana Garcia-Osta

PII: S0301-0082(20)30073-3

DOI: https://doi.org/10.1016/j.pneurobio.2020.101818

Reference: PRONEU 101818

To appear in: *Progress in Neurobiology*

Received Date: 16 January 2020

Revised Date: 27 March 2020

Accepted Date: 23 April 2020

Please cite this article as: { doi: https://doi.org/

Title: PLA2G4E, a candidate gene for resilience in Alzheimer´s disease and a new target for dementia treatment

Short running title: Role of PLA2G4E in Alzheimer´s disease

Authors:

Marta Perez-Gonzalez, [a,b,c] Maite Mendioroz, [c,d,e] Sara Badesso, [a,b,c] Diego Sucunza, [f,c] Miren Roldan, [c,d] Maria Espelosín, [a, c] Susana Ursua ,[a,c] Rafael Lujan, [g] Mar Cuadrado-Tejedor, [a,b,c*] Ana Garcia-Osta, [a,c*]

[a]Alzheimer´s disease, Neurosciences Program, Center for Applied Medical Research (CIMA), University of Navarra, Pamplona, Spain

[b]Department of Pathology, Anatomy and Physiology, School of Medicine, University of Navarra, Pamplona, Spain.

[c]IdiSNA (Navarra Institute for Health Research) Pamplona, Spain

[d]Neuroepigenetics Laboratory, Navarrabiomed, Public University of Navarra (UPNA), Pamplona, Spain.

[e]Department of Neurology, Complejo Hospitalario de Navarra, Pamplona, Spain.

[f]Parkinson´s disease, Neurosciences Program, Center for Applied Medical Research (CIMA), University of Navarra, Pamplona, Spain

[g]Synaptic Structure Laboratory, Instituto de Investigación en Discapacidades Neurológicas (IDINE), Departamento de Ciencias Médicas, Facultad de Medicina, Universidad Castilla-La Mancha, Campus Biosanitario, Albacete, Spain

*Correspondence and equall contribution:

Ana Garcia-Osta, PhD, agosta@unav.es

Mar Cuadrado-Tejedor, PhD, mcuadrado@unav.es

Highlights

- The study of cognitive resilient individuals represents a promising strategy to identify novel therapeutic targets for Alzheimer´s disease (AD).
- PLA2G4E is up-regulated in cognitive resilient Tg2576 mice.
- PLA2G4E loss is evident in the brain of late-stage AD patients
- Overexpression of PLA2G4E in aged-APP/PS1 mice restores spatial memory deficits.
- PLA2G4E represents a new therapeutic target to treat cognitive dysfunction

Abstract

Clinical studies revealed that some aged-individuals accumulate a significant number of histopathological Alzheimer´s disease (AD) lesions in their brain, yet without developing any signs of dementia. Animal models of AD represent suitable tools to identify genes that might promote cognitive resilience and hence, this study first set out to identify cognitively resilient individuals in the aged-Tg2576 mouse model. A transcriptomic analysis of these mice identified *PLA2G4E* as a gene that might confer resistance to dementia. Indeed, a significant decrease in PLA2G4E is evident in the brain of late-stage AD patients, whereas no such changes are observed in early stage patients with AD neuropathological lesions but no signs of dementia. We demonstrated that adeno-associated viral vector-mediated overexpression of PLA2G4E in hippocampal neurons completely restored cognitive deficits in elderly APP/PS1 mice, without affecting the amyloid or tau pathology. These PLA2G4E overexpressing APP/PS1 mice developed significantly more dendritic spines than sham-injected mice, coinciding with the cognitive improvement observed. Hence, these results support the idea that a loss of PLA2G4E might play a key role in the onset of dementia in AD, highlighting the potential of PLA2G4E overexpression as a novel therapeutic strategy to manage AD and other disorders that course with memory deficits.

Key words: Alzheimer´s disease, resilience, PLA2G4E, gene expression

1. Introduction

The progressive and irreversible cognitive impairment and memory loss that occurs in Alzheimer´s disease´s (AD), coupled to the presence of amyloid β (Aβ) peptide aggregates and neurofibrillary tangles (NFTs), constitute the main hallmarks of this disease (Serrano-Pozo et al., 2011). However, there is only a modest correlation between neuropathological lesions and the symptoms of dementia, and it is even possible to detect substantial AD lesions in the brain of cognitively normal elderly individuals (Savva et al., 2009; Brumback-Peltz et al., 2011; Bennett et al. 2012). In fact, a study published fifty years ago demonstrated amyloid plaques or NFTs in 13 of 14 brains from non-demented individuals older than 75 years-of-age (Tomlinson et al. 1968). More recently, large-scale epidemiological studies into healthy ageing and its association with longevity/neuropathology increased interest in cognitive resilience. For example, a post-mortem analysis identified amyloid plaques and NFTs in at least 12% of subjects over 75 years old with normal cognition (Tyas et al., 2007). This study demonstrated a significant impact of academic education and lifestyle in early life on cognitive status in the elderly (Iacono et al., 2009). Similar results were obtained in other longitudinal studies (O'Brien et al. 2009; White 2009; Lace et al. 2009), reinforcing the dissociation between AD lesions and cognition in the elderly (Ewbank and Arnold 2009; Haroutunian et al. 2008). Hence, classical AD hallmarks do not seem to be sufficient to predict dementia, raising the possibility of studying these asymptomatic AD individuals that normally escape the attention of medical researchers. Importantly, the mechanisms that underlie this cognitive resilience may reflect how the brain copes with the pathological markers of AD, possibly opening the way to find novel targets for AD treatment.

Most of the studies performed to identify factors associated with cognitive resilience in the context of AD have drawn attention to environmental factors like "cognitive reserve" (Stern, 2012) or specific lifestyles (exercise, diet, education…) as potential causes of such resilience (Bullain et al. 2013; Negash et al. 2013; Shlisky et al. 2017).

However, little attention has been paid to the biological events behind the failure to develop cognitive symptoms. Neuronal hypertrophy has been observed in AD resilient patients, suggesting it may constitute a compensatory mechanism against dementia through enhanced transcription of memory-related genes (Iacono et al., 2008). However, this study also suggested that altered gene expression may also protect against AD-associated cognitive deterioration. Moreover, an analysis of neuroinflammatory responses in post-mortem brains from resilient and demented individuals with AD lesions demonstrated that weaker glial activation, and different cytokine profiles, could influence the appearance of symptoms (Barroeta-Espar et al., 2019; Perez-Nievas et al., 2013).

However, the possibility of identifying the factors responsible for the protection against dementia in these subjects is hindered by: i) the intrinsic limitations of using post-mortem brain samples (Ferrer et al., 2008); ii) the genetic diversity of the individuals studied; and iii) the clinical, physical and lifestyle variation among subjects (Caspers et al., 2014). Thus, it may be necessary to take advantage of animal models to identify novel factors that might help to understand the molecular mechanisms underlying resilience. Indeed, genetic mechanisms of resilience discovered in animal models allowed a new target for Duchenne Muscular Dystrophy therapy to be identified (Vieira et al., 2015).

Therefore, we hypothesized that it might be possible to find some asymptomatic animals among the population of amyloid precursor protein (APP) Tg2576 transgenic mice, as occurs in humans. Here, we identified a subset of resilient 16-month-old (mo) Tg2576 mice (about 20%) who maintained their spatial memory intact, as evident in the Morris Water Maze test (MWM). The use of these resilient transgenic mice allowed us to minimize the environmental and genetic variants characteristic of human patients, facilitating the identification of causal factors of resilience. We found that the cytosolic phospholipase A2 Group IVE gene (*PLA2G4E*, also known as cPLA2ε), which has not been previously implicated in memory, is overexpressed in the brain of resilient Tg2576 mice, and that it is also downregulated when AD is associated with cognitive decline. Significantly, these data were consistent with that obtained in humans. Moreover, we also demonstrated that viral vector–mediated delivery of PLA2G4E to the hippocampus of aged APP/PS1 AD mice restored memory and increased dendritic spine density, suggesting an important role of this enzyme in synaptic plasticity and memory function.

2. Materials and methods

2.1. Animals

A group of aged (16-18 month-old) female transgenic Tg2576 mice, with an inbred C57BL/6/SJL genetic background, was used to identify cognitive resilient mice. This strain overexpresses hAPP with the Swedish (K670N/M671L) familial AD mutation under control of the prion promoter. Their negative littermates were also used in this study as a control group.

Two months-old male wild-type (WT) C57BL/6 mice, elderly male and female APP/PS1 mice and their negative littermates were also used to test the implication of PLA2G4E on cognitive function. The APP/PS1 model, which is on an inbred C57BL/6J genetic background, expresses human transgenes for the APP bearing the Swedish mutation and for the PSEN1 containing a L166P mutation, both driven by the Thy1 promoter.

Animals were housed 4–6 per cage with free access to food and water, and maintained in a temperature-controlled environment on a 12 h light–dark cycle. All procedures were carried out in accordance with the current European and Spanish regulations (2010/63/EU; RD52/2013) and the study was approved by the Ethical Committee of the University of Navarra (protocols no. 113-18).

2.2. Human AD samples and controls

Human brain samples used in this study were from the Navarra Health Service/Osasunbidea's Research Biobank and all the procedures were carried out in accordance with the Ethics Committee of the University of Navarra (protocol no. 2018.020).

Temporal cortex samples were obtained from patients which met the criteria for the diagnosis of Alzheimer-type pathology with an early-Braak stage (II-IV), for which no signs of dementia were reported at the age of death (n=9); AD patients with a late-Braak stage (V-VI) and dementia symptoms (n=9), and non-demented people with no AD pathology (n=8).

For all subjects, informed consent was obtained before the removal of brain tissue at death and subsequent use for research. Brain sections were stored at -80ºC until processing.

2.3. Generation of AAV2/9-hsynapsin-PLA2G4E virus

cDNA encoding full-length mouse phospholipase A2 group IVE (*Pla2g4E*) was isolated from the vector pRK5-PLA2G4E, kindly ceded by Dr. Cravatt (Ogura et al., 2016), and inserted into the multiple cloning site (MCS) of an rAAV2 plasmid that contained an hybrid human-synapsin (hsynapsin) promoter (kindly gifted by Dr. J. Gerez) and AAV2 inverted terminal repeats (ITRs), to obtain rAAV2-hsynapsin-PLA2G4E. Minipreps and maxipreps used to amplify the rAAV2-hsynapsin-PLA2G4E produced were prepared using commercial kits according to the manufacturer's instructions (Quiagen).

To produce the viral vector, recombinant single-stranded AAV2/9 vectors were purified from HEK-293T cells that had been co-transfected using linear polyethylenimine 25 kDa (Polysciences) with two different plasmids: one containing ITR-flanked transgene constructs (rAAV2-hsynapsin- *Pla2g4E*) and the other named pDP9 containing the adenoviral helper genes plus AAV2 rep and AAV9 cap, as described by Dr. Kamen's laboratory (Durocher et al., 2002). Supernatant was collected and treated with polyethylene glycol solution (PEG8000, 8% v/v final concentration) for 72 h at 4°C. It was then centrifuged at 1734 g for 15 min. Pellet containing particles from the supernatant was resuspended in lysis buffer (50 mM Tris-Cl, 150 mM NaCl, 2 mM $MgCl_2$, 0.1% Triton X-100) and kept at −80°C. Cells containing AAV particles were collected and treated with the same lysis buffer and maintained at -80ºC. Three cycles of freezing and thawing were applied to both supernatant and cell lysate. Viral particles obtained from cell supernatant and lysate were purified by ultracentrifugation in an iodioxanol gradient according to Zolotukhin's method (Zolotukhin et al., 1999). To further concentrate the viral batches, they were passed through Centricon tubes (YM-100, Millipore) and kept at -80ºC.

Viral titration, expressed as viral particles (vp)/ml, was obtained through quantitative PCR for viral genome copies extracted from DNAase-treated viral particles (High Pure Viral Nucleic Acid Kit, Roche). The primers used were: Forward- *Pla2g4E* 5′-

ATGGTGACAGACTCCTTCGAG -3′ and Reverse-*Pla2g4E* 5′-CCTCTGCGTAAAGCTGGTGG -3′ and the viral title obtained was 2.6 x 10^{11} vp/ml.

2.4. Stereotactic surgery for viral administration

Animals were anesthetized with an intraperitoneal dose of 80/10 mg/Kg of ketamine/xylazine and treated with the analgesic buprenorphine (Buprex) at a dose of 0.1 mg/Kg. Then, to overexpress PLA2G4E in hippocampal neurons, mice were bilaterally injected with 2.6 x 10^{8} genomic copies of the adeno-associated virus AAV2/9-hsynapsin-*PLA2G4E* (called from now AAV9-PLA2G4E) in the CA1 region of the hippocampus through a stereotactic surgery in the following coordinates: antero-posterior -2.0 mm; half-side ± 1.7 mm; dorso-ventral -2.0 mm (using bregma point as reference), using a 5 µl Hamilton syringe. Following the injection, the needle was left in place for 2 min, to avoid vector leakage, before withdrawing slowly the syringe. After surgery, animals were kept under constant monitoring with *ad libitum* access to food and water. Note that in this experiment, control mice were sham-injected.

2.5. Behavioral studies

All behavioral studies used in this study were carried out during light time, from 9:00 to 16:00 h.

2.5.1. Morris water maze test (MWM).

MWM test was used to select cognitive resilient mice and to test the effect of AAV-mediated PLA2G4E overexpression on spatial memory. During three consecutive days, mice underwent the visible-platform phase (eight trials per day) using a platform raised above the surface of the water and no visible cues. Mice that were able to perform the task in the same conditions undertook then the hidden-platform phase. In this phase, mice were trained during 5-7 consecutive days (four trials per day) to locate a platform submerged 1 cm beneath the water surface with the help of some visible cues present in the walls of the swimming pool. In both phases, mice were placed pseudo-randomly in selected locations and each trial was finished when the mouse reached the platform or after 60 s. After each trial, mice remained on the platform for 15 s. At different chosen days just before the hidden platform phase, mice were subjected to a probe trial (retention phase) in which they swam for 60 s in the pool without the platform. To identify cognitive resilient mice, a reversal MWM was carried out after 2 months

changing the location of the platform. All trials were monitored by a camera connected to a SMART-LD program (Panlab) for subsequent analysis of escape latencies during visible and hidden platform phases and percentage of time spent in each quadrant of the pool during the probe trials. All experimental procedures were performed blind to groups.

2.5.2. Fear conditioning test (FC).

FC paradigm was used to analyze the effect of PLA2G4E expression on fear memory. This behavioral test consists of three phases: habituation, training and test. It was carried out in a StartFear system (Panlab). During habituation phase, mice were habituated to the conditioning chamber for 3 min with no stimuli presented. After twenty-four hours, during the training phase, they were placed again in the same chamber and were allowed to explore for 2 min. After that, they received two footshocks (0.3 mA) of 2 s separated by an interval of 30 s and were returned to their home cages after another 30 s. The following day, mice were returned to the conditioning chamber and allowed to explore the context for 2 min. Freezing behavior was recorded during this time and freezing scores were expressed as percentages. The T24 group was sacrificed 24 h after the training and the TT group 1 h after the test. The naïve group was sacrificed without performing any step of the paradigm.

2.6. Determination of Aβ Levels

Parieto-temporal cortical Aβ_{42} levels were measured by using a sensitive sandwich ELISA kit (Invitrogen). Tissue was homogenized in a buffer containing 10 mM Tris-HCl ph=7.5, 1 mM NaF, 0.1 mM Na_3VO_4, 2% SDS and protease inhibitors. The homogenates were sonicated for 2 min, left 20 min on ice and centrifuged at 100 000 g for 1 h at 8ºC. The supernatant was directly diluted and loaded onto ELISA plates in duplicate. The assay was performed according to the manufacturer's instructions.

2.7. Dendritic spine density measurement by Golgi-Cox staining

In order to analyse dendritic spine density and morphology, a modified Golgi-Cox method was used (Glaser and Van der Loos, 1981). Half-brains were incubated in Golgi-Cox solution (1% potassium dichromate, 1% mercury chloride, 0.8% potassium chromate) for 48h at RT and protected from light. The solution was then renewed and

tissue was maintained there for another 3 weeks. After that, brains were washed with distilled water and maintained in 90º ethanol for 30 min. They were then processed in 200 μm-thick coronal slices using a vibratome. Slices were incubated in 70º ethanol, washed with distilled water, reduced in 16% ammonia for one hour and fixed in 1% sodium thiosulfate for 7 min. After another wash, slices were placed in microscope slides, dehydrated in an increasing alcohol graduation and mounted with DPX Mountant (VWR, BDH Prolabo).

Spine density was determined in the secondary apical dendrites of the pyramidal cells located within the CA1 region of the hippocampus. Each selected neuron was captured using a Nikon Eclipse E600 light microscope and images were recorded with a digital camera (Nikon DXM 1200F) at a resolution of 1,000-1,500 dots per inch (dpi). Secondary dendrites taken between 100-200 μm apart from the soma, where spine density is relatively uniform in CA1 pyramidal neurons (Megías et al., 2001), were used for the quantification. For each mouse (n=3-4 per group), 3 dendrites of 9 different neurons were used for the analysis.

2.8. Knocking down PLA2G4E in primary neuronal culture

We used specific small interfering RNA (siRNA) to inhibit PLA2G4E expression in primary neuronal cultures. To identify effective targeting sequences for RNAi, the full-length coding sequence of murine PLA2G4E was analysed using different algorithms. The efficiency of the candidate sequence to inhibit PLA2G4E expression was tested using SH-SY5Y cells co-transfected with a plasmid overexpressing murine PLA2G4E, that was kindly provided by Dr. Cravatt (Supplementary Figure 6). After probing a high efficacy to inhibit PLA2G4E expression, the candidate sequence was used to design shRNAs containing the H1 promoter, the 21 base sense and antisense sequences connected with a hairpin loop (TCAAGAGA) followed by a poly(T) termination signal (5´-
GTCGACTAATATTTGCATGTAGCTATGTGTTCTGGGAAATCACCATAAATGT
GAAATGTCTTTGGATTTGGGAATCTTATAAGTTCTGTATGAGACCACGGATC
CGGGTCTATGGTCTCCTTGTATCAAGAGTACAAGGAGACCATAGACCTTTTT
GGACCGGT) . The shRNA constructs were then cloned into an adeno-associated virus serotype 9 (AAV9) for stable siRNA delivery (Unitat de Producció de Vectors, Barcelona).

To evaluate the selective inhibition by PLA2G4E of activity-dependent signalling, we used primary neuronal cultures as a model to study synaptic responses by evoked bursts signals in functional neural networks. Primary neuronal cultures were obtained from the hippocampus and cortex of embryonic day 16 (E16) wild type (WT) mice (Ricobaraza et al., 2009) and infected with AAV9-shPLA2G4E or AAV9-shScrambled control on day in vitro (DIV) 1. Then, to trigger bursts of action potential firing, these cultures were treated at DIV 14 with bicuculline (50 μM, 1h), a GABA A receptor antagonist (Arnold et al., 2005) (Rao et al., 2006). Proteins were extracted in 2% SDS buffer and activation of CREB (phosphorylated at Ser133), pGluA1 and synapsin I expression were tested in lysates by immunoblot.

2.9. Mouse *PLA2G4E* promoter genotyping

To test whether differences in gene expression were related to specific genetic variability between mice, we screened *PLA2G4E* promoter region for sequence variation. Genomic DNA was isolated from mouse brain by salting out method. PCR primers were designed to amplify a 427-bp promoter region (chr2:120245023-120245449; GRCm38 mouse assembly) by using Primer3 Input (version 0.4.0) online software (Untergasser et al., 2012) as follows: Fw-5'-GGAAAGAGGTCACAGCTTCG-3' and Rev-5'-TGACCAGTCTCCACCATCAG-3'. Primer specificity was checked by in-silico PCR tool of UCSC Genome Browser GRCm38/mm10 mouse assembly. PCR was performed with GoTaq® DNA polymerase (Promega, Madison, WI, USA). Specificity of PCR reaction was assessed by running 5μl of PCR product on a 0.8% agarose gel to visualize a single 427-bp band. Next, PCR product was purified with PureLink® PCR Purification Kit ((Invitrogen, ThermoFisher Scientific) and subjected to Sanger sequencing. Forward and reverse sequences for each sample were obtained. dbSNP (version 142) was used to identify genetic variants. Poly Peak Parser tool was utilized to facilitate identification of the different alleles for heterozygous indel variant (Hill et al., 2014) . Statistical analysis was performed using GraphPad Prism version 6.01 (Graph Pad Software Inc., San Diego, CA, USA).

2.10. Immunofluorescence

Primary neuronal cultures were obtained from the hippocampus and cortex of embryonic E16 WT mice (Ricobaraza et al., 2009) and neurons were fixed at DIV 14

with 4% paraformaldehyde (PFA) and 4% sucrose in PBS during 8 minutes. Next, neurons were permeabilized with 0.1% Tx-100 in PBS for 20 min at RT and then blocked for 1 h with normal goat serum (NGS) and BSA (3% each) in PBS. Cells were incubated with primary antibodies (mouse anti-MAP2, 1:2000 from Sigma-Aldrich and rabbit anti-PLA2G4E, 1:500 from Proteintech) for 2 hours at RT. After washing and incubating for other 2 hours at RT with the corresponding secondary antibodies, they were washed again with PBS and finally stained for DAPI (Sigma-Aldrich, 1:50,000) during 5 min. The coverslips were placed on microscope slides on an 8-µL drop of mounting medium (DABCO; Sigma) and dried for 30 min at 37° C.

2.11. Immunohistochemistry

Brain mice hemispheres were immersion-fixed in paraformaldehyde and cryopreserved in 30% sucrose at 4ºC. Coronal microtome sections (30 µm thick) were collected and stored at -20ºC until use. Brain slices were incubated in blocking solution (PBS containing 0.5% Triton X-100, 0.1% BSA and 2% NGS) for 2 h at room temperature. Sections were then incubated for 24 h at 4ºC with one of the following antibodies diluted in blocking solution: mouse monoclonal 6E10 (against amino acids 1-17 of Aβ peptide, 1:1000, BioLegend, San Diego, CA, USA) or mouse monoclonal anti-phospho-Tau (Ser202/Thr205) AT8 (1:50: Pierce Biotechnology Inc.). For 6E10 immunostaining, brain sections were incubated in 70% formic acid for 7 min to expose the epitope prior to incubation with the antibody. After washing with PBS, the brain sections were incubated with the secondary polyclonal goat anti-mouse biotinylated antibody (1:500, Dako) for one hour and then with horseradish peroxidase (HRP)-labeled Vectastain Elite ABC kit (Vector Laboratories). The peroxidase reaction was visualized with 0.05% 3-3′-diaminobenzidine tetrahydrochloride (DAB, Vector Laboratories) in PBS. Sections were then mounted on gelatin-coated slides, air-dried, dehydrated in graded ethanol solutions, cleared in xylene and cover-slipped with DPX mounting medium (BDH Chemicals Ltd.).

Images were analyzed with ImageJ software and the amyloid burden, defined as the total percentage of area covered by amyloid deposits over three sections, was calculated for hippocampus.

An immunohistochemistry was performed in formalin-fixed paraffin-embedded human hippocampal sections to detect PLA2G4E inclusions using a rabbit-polyclonal

antiserum (Proteintech; diluted 1:100). Antibody binding was then detected using the EnVision+ System-HRP labeled polymer (Dako) and DAB as chromogen. After immunostaining, sections were counterstained with hematoxylin–eosin and protein immunoreactivity was finally assessed under a light microscope (BX51, Olympus).

2.12. Thioflavin T staining

Compact senile plaques were detected in PFA immersion-fixed half-brains by Thioflavin T staining. Brain slices were first placed on the slides and dried for 24 h at RT. Afterwards, they were incubated in Mayer's hematoxylin solution (Sigma) for 3 minutes and washed in distilled water. After that, they were treated with 1% Thioflavin for 3 min, washed again with distilled water and incubated for 10 min in 1% acetic acid. Finally, brain slices were dehydrated in toluene and mounted using Immu-Mount™ (Thermo Fisher Scientific). An automated microscope (Zeiss Axioplan 2ie) was used to analyse fluorescence signals. Images were analyzed with ImageJ software and the amyloid burden, defined as the total percentage of area covered by amyloid deposits over three sections, was calculated for hippocampus.

2.13. Protein extracts

To obtain total protein extracts, brain samples were homogenized in lysis buffer with protease inhibitors (10 mM Tris-HCl ph=7.5, 1 mM NaF, 0.1 mM Na_3VO_4, 2% SDS), sonicated for 2 min, left 20 min on ice and centrifuged at 15700 g for 13 min at 8ºC. The supernatant was stored at -80ºC. Total protein concentrations were determined using the Pierce™ BCA Protein Assay kit (Thermo Scientific).

In case of human tissue, to get synaptosome-enriched protein extracts, tissue was homogenized in a buffer containing Syn-PER (Thermo Fisher Scientific), a commercial proteases inhibitors cocktail (Sigma P8340) and two commercial phosphatases inhibitors (SigmaP5726 and SigmaP0044). Homogenates were then centrifuged for 15 min at 1000 g and 4ºC and the supernatants were kept and centrifuged again for 20 min at 15000 g and 4ºC. The supernatants obtained in this second centrifugation constitute the cytosolic fraction. The pellets were re-suspended in a solution containing 1% sodium deoxycholate, a proteases inhibitors cocktail (Sigma P8340) and phosphatases inhibitors (SigmaP5726 and SigmaP0044) diluted in PBS. Thereafter, they were sonicated in 20 pulses and centrifuged for 20 min at 15000 g and 4ºC. The supernatants

obtained constitute the synaptosome-enriched fraction and were kept at -80ºC until used. Protein concentration was obtained using the Pierce BCA Protein Assay kit (Thermo Fisher Scientific).

2.14. Immunoblotting

For APP-derived fragments (C99 and APP) analysis, the parieto-temporal cortex extracts used for determining Aβ levels were mixed with 4x XT sample buffer (Bio-Rad), boiled for 5 min at 95 ºC, resolved onto a Criterion™ XT precast gel 4-12% Bis-Tris (Bio-Rad) using XT MES (Bio-Rad) running buffer and transferred to nitrocellulose membranes.

In the rest of cases, protein samples were mixed with 6x Laemmli sample buffer, boiled for 5 min at 95 ºC, resolved onto SDS-polyacrylamide gels and transferred to nitrocellulose membranes.

In all cases, membranes were then blocked with 5% milk in TBS and incubated overnight with the following primary antibodies: mouse monoclonal 6E10 (reactive to amino acids 1–17 of Aβ peptide, 1:1000, BioLegend), mouse monoclonal anti-p-Tau AT8 (1:1000, Thermo Fisher Scientific), rabbit polyclonal anti-pGluA1-Ser831(1:1000, Millipore), rabbit polyclonal anti-GluN2B (1:1000, Upstate), mouse monoclonal anti-PSD95 (1:1000, Chemicon), mouse monoclonal anti-pCaM Kinase II (Thr286) (α subunit, clone 22B1, 1:1000, Upstate), mouse monoclonal anti-synaptophysin (1:1000, Millipore), rabbit monoclonal anti-pCREB (Ser133) (1:1000, Cell Signaling), rabbit polyclonal anti-pGSK3β (Ser9) (1:1000, Cell Signaling), mouse monoclonal anti-synapsin I (1:1000, Synaptic Systems), rabbit polyclonal anti- PLA2G4E (1:1000, Proteintech) and mouse monoclonal anti-β-actin (1:100000, Synaptic Systems) in the corresponding buffer. After two washes in TBS/Tween-20 and one in TBS alone, immunolabeled protein bands were detected with an HRP-conjugated anti-rabbit or anti-mouse antibody (1: 5000, Santa Cruz). Antibody binding was then visualized by enhanced chemiluminescence system (ECL, GE Healthcare Bioscience), and autoradiographic exposure to Hyperfilm™ ECL (GE Healthcare Bioscience). Quantity One™ software v.4.6.3 (Bio-Rad) was used for protein quantification.

2.15. Affymetrix Microarray Hybridization and Data Analysis

RNA was extracted from hippocampus obtained from Imp_Tg2576 (n=4) and Res_Tg2576 (n=4) using Trizol Reagent (Sigma-Aldrich) and its integrity was confirmed on Agilent RNA Nano LabChips (Agilent Technologies). The sense cDNA was prepared from 300 ng of total RNA using the Ambion WT Expression Kit. The sense strand cDNA was fragmented and biotinylated using the Affymetrix GeneChip WT Terminal Labeling Kit (PN 900671). According to the manufacturer's instructions, labeled sense cDNA was hybridized to the Affymetrix Mouse Gene 2.0 ST microarray and with the GeneChip Hybridization, Wash, and Stain Kit. Genechips were scanned with the Affymetrix GeneChip Scanner 3000. Background correction and normalization were done using RMA (Robust Multichip Average) algorithm (Irizarry et al., 2003) and a filtering process was performed to eliminate low expression probe sets. R/Bioconductor (Gentleman et al, 2006) was used for preprocessing and statistical analysis. LIMMA (Linear Models for Microarray Data) (Smyth, 2004) method was used first to find out the probe sets that showed significant differential expression between experimental conditions, selecting genes as significant using p-value<0.01 as threshold. False Discovery Rate (FDR) method was also use to correct for multiple hypotheses testing and finally the Ingenuity Pathway Analysis software (Ingenuity Systems, www.ingenuity.com) was used to check altered metabolic pathways between groups.

2.16. Quantitative real-time PCR

Total RNA was isolated from the correspondent mice or human tissue using Trizol reagent (Sigma-Aldrich). The RNA was treated with DNase at 37ºC for 30 min and reverse-transcribed into cDNA using SuperScript® III Reverse Transcriptase (Invitrogen).

Quantitative real-time PCR was performed to quantified gene expression. For *Pla2g4E* expression, assays were done using Power SYBR Green PCR Master Mix (Applied Biosystems) and the corresponding specific primers for *PLA2G4E* (Fw: 5'ATGGTGACAGACTCCTTCGAG 3', Rev: 5'CCTCTGCGTAAAGCTGTGG 3') and for the internal control *36B4* (Fw: 5'AACATCTCCCCCTTCTCCTT 3', Rev: 5' GAAGGCCTTGACCTTTTCAG 3'). Real-time was carried out using an ABI Prism 7300 sequence detector (Applied Biosystems) and data were analyzed using the Sequence Detection software v.3.0 (Applied Biosystems). The relative gene expression was calculated with reference to the control group using the DDCT method (Livak and

Schmittgen, 2001). For the glial fibrillary acidic protein (*GFAP)* and *CD11b* genes, TaqMan probe was employed with specific primers (FAM reporter), reference Mm01253023_m1 for *GFAP* and Mm00434455_m1 for *CD11b* (Thermo Fisher Scientific). *β-actin* was used as reporter gene (VIC reporter, reference Mm00607939_s1). In every case, PCR experiments were done in triplicate using samples of WT (n=5), Imp_Tg2576 (n=4) and Res_Tg2576 (n=4).

2.17. Pre-embedding immunogold electron microscopy

Immunohistochemistry for electron microscopy was performed using the pre-embedding immunogold technique as previously described (Luján and Shigemoto, 2006). Mice were deeply anesthetized and perfused with 4% paraformaldehyde and 0.05% glutaraldehyde in 0.1 M phosphate buffer (PB, pH=7.4). Brains were then immersed in the same fixative for 2 h and they were processed in 60 μm-thick coronal sections using a vibratome. Sections were incubated with 3-5 μg/ml of the primary antibody PLA2G4E (Proteintech) in TBS containing 1% NGS for 24 h at 4ºC. After being washed with TBS, sections were incubated for 2h in goat anti-rabbit IgG coupled to 1.4 nm gold (Nanoprobes Inc.) diluted 1:100 in TBS containing 1% NGS. After several washes in PBS, sections were postfixed in 1% glutaraldehyde dissolved in PBS. They were washed in double distilled water, followed by silver intensification through an HQ silver kit (Nanoprobes Inc.). The labelled sections were then treated with OsO_4 (1% in 0.1 M PB), block-stained with 1% uranyl acetate, dehydrated in a graded series of ethanol and flat-embedded on glass slides in Durcupan resin (Fluka). Regions of interest were cut at 70–90 nm on an ultramicrotome (Reichert Ultracut E, Leica) and collected on single slot pioloform-coated copper grids. Staining was performed on drops of 1% aqueous uranyl acetate followed by Reynold's lead citrate. Ultrastructural analyses were performed in a JEOL-1010 electron microscope.

2.18. Data and statistical analyses

The results were processed for statistical analysis using GraphPad PRISM, version 5.03. Unless otherwise indicated, results are presented as mean ± standard error of the mean (SEM). Normal distribution of data was checked by the Shapiro–Wilk test. Unpaired two-tailed Student's *t*-test was used to compare two groups and one-way ANOVA followed by Newman-Keuls Multiple comparison *post hoc* test to compare more than two groups. In the MWM test, latencies to find the platform were analyzed by two-way

repeated measures ANOVA test (genotype x trial) followed by the Bonferroni's *post hoc* test to compare cognitive status among groups. Statistical significance was set at *$P \leq 0.05$ or **$P \leq 0.01$.

3. Results

3.1. Identification of aged-Tg2576 resilient mice

To determine if cognitive resilience to AD lesions also occurs in Tg2576 mice, spatial memory was evaluated in a cohort of 14-16 mo Tg2576 mice (n=26) and their wild-type (WT) littermates (n=30) in the MWM test. To compare animals that performed similarly, mice that presented escape latencies longer than 15 s in the last block of visible platform training were excluded. While 30% of Tg2576 and 27% of WT mice did not comply with these criteria, a cohort of Tg2576 (n=18) and WT (n=22) mice was established with similar escape latencies in the visible-platform phase (Fig. 1A) or on the first day of the hidden-platform (Fig. 1B). As expected, Tg2576 mice behave significantly worse in the hidden-platform phase than WT mice (effect of day $F(4,190) = 268.0$, $P < 0.0001$; effect of genotype $F(1,190) = 160.81$, $P < 0.0001$; day × genotype interaction $F(4,190) = 15.69$, $P < 0.0001$ two way ANOVA with repeated measures: Fig. 1B), confirming the spatial memory deficit associated with this AD mouse model from 12 months of age (Hsiao et al., 1996). However, when the data were analyzed individually, we found that 4 of the 18 Tg2576 mice (22%) showed similar behavior to WT mice. To confirm this unexpected behavior, a reversal MWM test was performed on the 4 resilient mice (Res_Tg2576) two months later, when the AD phenotype is known to be well-established in this mouse model, and on 4 Tg2576 mice with spatial memory impairment (Imp_Tg2576) and 5 WT mice. Again, Res_Tg2576 mice showed similar escape latencies to WT mice and significantly lower than the Imp_Tg2576 mice in the hidden-platform phase of the reversal MWM test (effect of day $F(2,40) = 67.62$, $P < 0.0001$; effect of group $F(3,40) = 57.69$, $P < 0.0001$; day × group interaction $F(6,40) = 7.91$, $P < 0.0001$ two way ANOVA with repeated measures: Fig. 1C). Moreover, in the retention-phase carried out on the 5^{th} day (probe trial), Res_Tg2576 mice spent significantly more time in the correct quadrant than Imp_Tg2576 mice (one-way ANOVA with group as variable $F(2, 10)= 36.14$, $P < 0.0001$: Fig. 1D), confirming their better cognitive performance. To note, Res_Tg2576 performed the probe trial slightly worse than WT mice ($P < 0.05$: Fig. 1D).

3.2. Increased expression of synaptic markers in aged-Tg2576 resilient mice independent of amyloid burden, tau pathology and neuroinflammation

The accumulation of amyloid and tau, together with synaptic dysfunction, constitute the main pathological markers of AD (Serrano-Pozo et al., 2011). To analyze amyloid pathology, APP processing was analyzed in immunoblots of SDS extracts of the parieto-temporal cortex, yet no significant differences were found between Res_Tg2576 and Imp_Tg2576 mice (Supplementary Fig. 1A). Soluble $A\beta_{42}$ was assayed in the same extracts by ELISA and again, there were no clear differences between these groups of mice ($t=0.444$, $P=0.6724$: Fig. 2A). Moreover, staining with the 6E10 antibody (Supplementary Fig. 2A, B) and thioflavin T (Supplementary Figure 2C, D) identified no significant differences in the number of immature and mature senile plaques between both groups of mice. Hence, the amyloid pathology in the Imp_Tg2576 and Res_Tg2576 mice had a similar status. Next, tau pathology was then analyzed since, although the Tg2576 mouse model is most frequently used to study the amyloid pathology in relation to AD, a significant increase of tau hyperphosphorylation is evident in these mice from 12 months of age (Puig et al., 2004). First, the accumulation of ptau (Ser202/Thr205) and pGSK3β-Ser9 (the inactive form of the main kinase responsible for tau phosphorylation) was explored in immunoblots of pre-frontal cortex SDS extracts. While no significant differences in ptau accumulation were observed in SDS extracts (one way ANOVA with group as variable $F(2,10)=1.203$, $P<0.3404$: Figure 2B), there was a pronounced decrease in pGSK3β-Ser9 in both groups of Tg2576 mice relative to the WT mice (one way ANOVA with group as variable $F(2,10)=10.47$, $P<0.001$: Figure 2C). Tau hypephosphorylation accumulation was however clearly observed when hippocampal sections of Imp_Tg2576 and Res_Tg2576 were stained with AT8 antibody. As depicted in Supplementary Fig. S3, immunoreactive processes and dystrophic neurites that seem to surround amyloid cores were present in both Tg2576 groups, whereas were absent in WT mice.

To assess whether a diminished neuroinflammatory response might underlie the resilience in Tg2576 mice, as suggested in humans (Barroeta-Espar et al., 2019; Perez-Nievas et al., 2013), we measured the levels of *GFAP* and CD11 expression, markers of astrogliosis and microgliosis, respectively. While *GFAP* was expressed more strongly in the transgenic mice than in the WT mice (one way ANOVA with group as variable

F(2,10)=8.401, P < 0.01), this expression did not differ between the cognitively resilient and impaired Tg2576 mice (Fig. 2D). Conversely, the *CD11b* expression was similar in all the mice tested (one way ANOVA with group as variable F(2,10)=2.579, P = 0.1250: Fig. 2D). Hence, differences in astrogliosis or microgliosis do not appear to explain the resilience observed in some of the Tg2576 mice.

We then assessed if the expression of molecules that play a critical role in memory formation may differ among these mice. The phosphorylated cAMP response element binding protein (pCREB), an important transcription factor, and other synaptic proteins were studied in immunoblots of pre-frontal cortex extracts, and interestingly, there was significantly more pCREB in the Res_Tg2576 GL mice than in the other two groups (one way ANOVA with group as variable F (2,10)=12.92, P<0.001: Fig. 2E). Likewise, the extracts from these mice contained more of the presynaptic marker synapsin I (one way ANOVA with group as variable F (2,10)=7.931, P<0.001: Fig. 2F) and the postsynaptic marker PSD95 (one way ANOVA with group as variable F (2,9)=0.5350, P<0.05: Fig. 2G). Taking into account that several studies have shown increased pCREB levels following training on memory tasks such as the MWM (Porte et al., 2008b), these data correlated with the better spatial memory observed in the Res-_Tg2576 mice compared to the Imp_Tg2576. Surprisingly, despite the differences observed in behavior, there were no longer differences in pCREB levels between WT and "conventional" impaired transgenic mice. These data are in accordance to different studies showing, in WT animals, age-related defects in spatial memory associated to a reduction in CREB activation following training sessions (Porte et al., 2008a). However, as described by Westerman et al., in this case WT aged-animals were able to learn the task properly after several MWM-training sessions (Westerman et al., 2002). Regarding Imp_Tg2576 mice, beyond the effect of aging, AD-related pathology imped them learn accurately. Significant differences between WT and both groups of transgenic mice were observed when levels of GluN2B (one way ANOVA with group as variable F(2,10)=32.88, P<0.0001) and pGluA1 (one way ANOVA with group as variable F(2,10)=25.10, P<0.0001) were analyzed in the same extracts (Fig. 2G). Considering that Imp_Tg2576 and Res_Tg2576 mice show similar amyloid levels (Fig. 2A), these results, are in accordance with several studies showing that Aβ levels influence AMPA and NMDA glutamate receptors in the brain (Guntupalli et al., 2016).

Finally, to further explore the mechanism underlying the improvement in memory function, we analyzed the levels of phosphorylation of calcium/calmodulin-dependent protein kinase II (pCaMKII; Thr286) that may also promote synaptic plasticity (Giese and Mizuno, 2013). Interestingly, although no significant differences were observed among groups, both WT and Res_Tg2576 mice, with a better performance in the MWM, showed similar and much higher levels of pCAMKII than Imp_Tg2576 mice (Fig. 2G).

3.3. Cognitive resilience to AD pathology is promoted by PLA2G4E

In light of these data, an Affymetrix Microarray was interrogated to analyze the hippocampal transcriptome and to identify genes differentially expressed between the resilient (n=4) and the impaired (n=4) Tg2576 mice. A LIMMA analysis was used to identify the probe sets that showed significant differential expression between the two experimental groups (Smyth, 2004) and genes were selected using a $P<0.01$ threshold of significance. These results are available to the community via GEO (under accession number GSE147434). Of the genes differentially expressed (Supplementary Table 1), *PLA2G4E* displayed the strongest fold change (log fold change = 0.97) and it was more intensely expressed by the Res_Tg2576 mice. This increase in *PLA2G4E* expression was validated by RT-PCR ($t=7.076$, $P<0.0001$, n=4 per group: Fig.3A).

The PLA2G4E protein was examined in immunoblots of parieto-temporal (Fig. 3B) and prefrontal cortex SDS extracts (Supplementary Fig. 4), and consistent with the mRNA expression data, there appeared to be more PLA2G4E protein in Res_Tg2576 extracts from both regions than in Imp_Tg2576 mice, although this increase did not reach statistical significance (parieto-temporal cortex, $F(2,10)=2.286$, $P=0.1522$, Fig. 3B; and pre-frontal cortex $F(2,9)=1.275$, $P=0.3254$ one way ANOVA with group as variable: Supplementary Fig. 4). It was also noteworthy that less PLA2G4E protein was detected in the Imp_Tg2576 mice than in the WT mice, suggesting that this enzyme might be down-regulated in AD.

These data were confirmed in a new batch of aged Tg2576 animals that underwent the same behavioral tests to obtain a greater number of resilient mice (Supplementary Fig. S5A,B). PLA2G4E expression was significantly enhanced in the hippocampal protein extracts obtained from Res_Tg2576 mice relative to the impaired Tg2576 group (t test, $p< 0.05$, n=3-4) (Supplementary Fig. S5C).

To validate these findings in humans, we analyzed PLA2G4E expression in temporal cortex brain samples from: i) AD patients at an early Braak stage (II-IV) with pathological amyloid and tau in their brain but no symptoms of dementia (Supplementary Table 2); ii) AD patients at a late Braak stage (V-VI) with more pathological amyloid and tau in the brain and cognitive impairment (Supplementary Table 3); and a iii) control group with no evidence of pathological amyloid or tau in their brain (Supplementary Table 4). PLA2G4E and the synaptic marker synapsin I were analyzed in cytosolic- and synaptosomal-enriched protein extracts respectively, and in western blots, less PLA2G4E (one way ANOVA with group as variable $F(2,23)=5.652$, $P<0.05$, Fig. 3C) and synapsin I (one way ANOVA with group as variable $F(2,22)=1.402$, $P=0.2672$, Fig. 3D) were detected in the V-VI AD patients relative to the controls. However, there were similar levels of both PLA2G4E and synapsin I to those of controls in AD II-III patients with no evidence of cognitive deficits. These data support the hypothesis that the loss of PLA2G4E might play a key role in AD progression and/or in the onset of signs of dementia.

3.4. Differences in *PLA2G4E* expression are associated with promoter variation

We next evaluated whether differences in *PLA2G4E* expression might be associated with genetic variability in the promoter region of the gene. Primers were designed to amplify a 427 bp promoter region by PCR (Fig. 4A) and when genomic DNA from the brains of 16 mice were analysed by PCR (Res_Tg2576, n=8; Imp_Tg2576, n=8), Sanger sequencing revealed the presence of a 13 bp deletion (-/GACTGCGCCGCCG) in the 5'UTR of *PLA2G4E* that involved part of a repetitive CpG element (Fig. 4B). This 13 bp deletion was not registered in dbSNP v142, yet it includes a rare 6 bp in-frame deletion (-/CGCCGC) variant referred to as rs226296356 in dbSNP v142. When the allele frequency distribution for the 13 bp deletion was compared between resilient and impaired mice, a chi-squared test showed the 13 bp deletion allele to be more frequent among the Res_Tg2576 mice ($P<0.05$, Fig. 4C). Using the MotifScan prediction software (Aerts et al., 2003), we identified a new binding site for the transcriptional activator Specificity Protein 1 (SP1) in the 5'UTR promoter sequence that is generated by this 13 bp deletion. The presence of SP1 may contribute to the increase PLA2G4E expression.

3.5. Neuronal PLA2G4E localized mainly in the cytosol but it is also present in dendrites and dendritic spines

It has been reported that in the brain, PLA2G4E is distributed in neurons (Ogura et al., 2016). We confirmed that PLA2G4E was expressed strongly by cortical and hippocampal neurons in primary cultures from mice foetuses on E16 where it co-localized with MAP2 (Fig. 5A). Immunohistochemistry on formalin-fixed paraffin-embedded hippocampal sections from human showed that immunoreactivity for PLA2G4E was mainly located in the cytoplasm of cells bodies of hippocampal neurons(Fig. 5B), and less frequently associated with apical dendrites connected to their parent cell bodies (Fig. 5B, black arrow). The subcellular distribution of PLA2G4E was further characterized in the CA1 region of mouse hippocampus using the pre-embedding immunogold technique (Luján and Shigemoto, 2006). PLA2G4E immunoparticles were mostly found at the dendrites (Den) of pyramidal cells (arrows, left panel Fig. 5C), and on the extrasynaptic plasma membrane (s) of the dendritic spines that establish excitatory synapses with axon terminals (at, arrows, right panel). A few immunoparticles were also observed at intracellular sites (crossed arrows) in dendritic spines (s).

3.6. The up-regulation of PLA2G4E expression is induced after Fear Conditioned memory retrieval, suggesting its involvement in memory function

The neuronal location of PLA2G4E at the synapse, together with its up-regulation in the brain of cognitive resilient subjects, suggested that this enzyme might play a role in memory. To obtain more direct evidence of a functional role of PLA2G4E in learning and memory, we tested whether PLA2G4E expression was regulated in the fear conditioning (FC) test. This task requires hippocampal-dependent transcription and protein synthesis, and it has been widely used to characterize the biochemical requirements for memory formation (Huff et al., 2006). pCREB and PLA2G4E expression in the brain was analysed in immunoblots after fear-memory consolidation in 2-month-old C57BL/6J WT mice sacrificed one hour after being tested in the FC paradigm (TT group; n=8), and it was compared to that of mice sacrificed 24 h after the training phase of FC (T24 group; n=7) and to that of mice that were not subjected to any aspect of the FC test (naive group; n=8). As expected, there was a significant increase

($P < 0.001$) in freezing time (indicative of memory formation) among the mice re-introduced into the cage (TT group) during the test phase relative to that of the training phase (Fig. 6A). As CREB-mediated transcription is necessary for consolidation and reconsolidation of contextual fear memory (Kida et al., 2002) , pCREB was first analyzed as indicative of neural plasticity in both the hippocampus and prefrontal cortex of mice). In TT mice, there was an up-regulation of pCREB in the hippocampus (one way ANOVA with group as variable, $F(2,32)=6.240$, $P\leq0.01$; Fig. 6B) and also a tendency was observed in the prefrontal cortex (one way ANOVA with group as variable, $F(2,32)=2.554$, $P=0.0935$, Supplementary Fig. S6A). PLA2G4E expression was also stronger in both of these areas in the TT mice than in the T24 and naive groups, although the difference was not significant in the hippocampus (one way ANOVA with group as variable, hippocampus: $F(2,22)=5.964$, $P=0.0594$, Fig. 6C; prefrontal cortex $F(2,20)=5.964$, $P<0.001$;Supplementary Fig. 6B). These data suggest that there is an increase in PLA2G4E in the hippocampus and cortex during contextual memory retention, after the retrieval of a consolidated memory.

3.7. The knockdown of PLA2G4E blocks the activation of synaptic proteins involved in synaptic transmission

Considering the plausible role of PLA2G4E in memory function, *in vitro* assays were conducted to further characterize its role on synaptic activity. For this purpose, we used a well-characterized protocol in cortical and hippocampal primary neurons based on the exposure to the GABA(A) receptor antagonist bicuculline (50 μM, 1 hour) which is able to induce and/or increase synaptic efficacy at excitatory synapses (Rao et al., 2006). First, to demonstrate NMDA receptor activation, CREB activation (phosphorylation of CREB at the activator site residue Ser 133) was analysed (Ginty et al., 1993). As depicted in Figure 6D, and described by several authors (Hardingham et al., 2002), we demonstrated that bicuculline (through the activation of NMDA receptors) caused a sustained CREB phosphorylation at Ser133 (one way ANOVA, $(3,14) = 38.59$, ***$P<0.0001$ control vs bicuculline) as well as an increase of AMPA receptor activation (Rao et al., 2006) which was analysed measuring pGluA1 levels (one way ANOVA, $(3,14) = 13.61$, ***$P<0.0001$ control vs bicuculline). Furthermore, synapsin I levels were also analysed since this presynaptic protein increases in the hippocampus during long term potentiation (LTP) (Sato et al., 2000) and plays a fundamental role in the

formation, maintenance and rearrangements of synaptic contacts (review in Cesca et al., 2010). A significant increase of synapsin I was also observed in neuronal cultures activated with bicuculline (one way ANOVA, (3,10) = 11.65, **P<0.001 control vs bicuculline). PLA2G4E expression was next analysed on the same conditions and, interestingly, we observed that it was strongly induced by bicuculline (one way ANOVA, (3,14) = 14.16, ***P<0.0001 control vs bicuculline) (Fig. 6D) which indicates that neuronal activation indeed upregulated PLA2G4E expression.

We then analysed the effect of chronic PLA2G4E knockdown using an AAV-PLA2G4E-shRNA. First, we demonstrated that our AAV-PLA2G4E-shRNA blocked PLA2G4E expression in a system of SH-SY5Y cells expressing murine PLA2G4E (Supplementary Fig. S7). Next, in neuronal pprimary cultures we demonstrated that the treatment with AAV-PLA2G4E-shRNA blocked PLA2G4E-induced by bicuculline (one way ANOVA, $$$ P<0.0001, bicuculline vs AAV-PLA2G4E-shRNA and bicuculline) and effectively blocked the activation of CREB (one way ANOVA, $$$ P<0.0001 bicuculline vs AAV-PLA2G4E-shRNA and bicuculline) and GluA1 (one way ANOVA, $$ P<0.001 bicuculline vs AAV-PLA2G4E-shRNA and bicuculline) driven by bicuculline (Fig. 6D). Likewise, acute PLA2G4E knockdown no longer increased synapsin I expression in response to bicuculline (one way ANOVA, $ P<0.05 bicuculline vs AAV-PLA2G4E-shRNA and bicuculline), suggesting that synapse formation and/or stability may be altered upon PLA2G4E knockdown.

3.8. AAV-mediated overexpression of hippocampal PLA2G4E restores memory deficits in aged-APP/PS1

To validate PLA2G4E as potential new therapeutic target, we used a slightly different AD model to the Tg2576 mice in which PLA2G4E was identified, enhancing the potential and confidence in PLA2G4E as a therapeutic target. Interestingly, we found that PLA2G4E expression was also dysregulated in the APP/PS1 AD model, which develops the amyloid pathology earlier than in Tg2576 mice. In the hippocampus of APP/PS1 mice there was less PLA2G4E mRNA after disease onset than in their transgene-negative littermates (at 6 mo, P = 0.076; and 11 mo, P = 0.053: Supplementary Fig. 8). Thus, to confirm the effect of PLA2G4E on memory function and to analyse its potential as a novel therapy for AD, this enzyme was overexpressed in

the hippocampal neurons of elderly APP/PS1 mice (16-19 mo) using an adeno-associated virus (AAV).

Two months after viral injection, the memory capacity of APP/PS1 AAV injected mice (APP/PS1 AAV9-PLA2G4E, n=10) was assessed in the MWM test, and compared with that of sham-injected APP/PS1 (APP/PS1 sham, n=9) mice and their transgene-negative littermates (n=9). During the visible-platform phase, the escape latencies of both groups of APP/PS1 mice were significantly longer than those of the WT animals on days 1 and 2, demonstrating a significant main effect of genotype (two way ANOVA with repeated measures effect of day $F(2,57) = 43.96$, $P < 0.0001$; effect of group: $F(2,57) = 15.57$, $P < 0.0001$; day × group interaction, $F(4,57) = 0.69$, $P = 0.5993$: Fig. 7A). However, no significant differences were observed among the groups in the last trial, indicating that all animals were able to perform the task in the same conditions. As expected, sham APP/PS1 mice behaved significantly worse than WT mice in the hidden-platform phase (Fig. 7B), confirming the impaired spatial memory associated with this AD mouse model (Serneels et al. 2009). Interestingly, the escape latencies of the AAV9-PLA2G4E mice were similar to those of the WT mice, indicating that hippocampal PLA2G4E overexpression rescued the spatial working-memory impairment of the APP/PS1 mice (two way ANOVA with repeated measures effect of day $F(6,147) = 2.96$, $P < 0.05$; effect of group: $F(2,147) = 27.22$, $P < 0.05$; day × group interaction, $F(12,147) = 0.98$, $P = 0.4717$: Fig. 7B). Moreover, PLA2G4E overexpression also enhanced memory retention in the probe trials performed on days 6 (one way ANOVA effect of group for the 60 second probe, $F(2,21)=6.854$, $P < 0.001$: Fig. 7C) and 8 (one way ANOVA effect of group for the 60 second probe, $F(2,21)=3.646$, $P < 0.05$: Figure 7C) of the hidden-platform phase of the test. Hence, PLA2G4E overexpression or the stimulation of its activity appears to be a potentially promising strategy to manage AD.

The viral expression of PLA2G4E was verified by both PCR and in western blots of hippocampal tissue from a representative number of mice injected with the AAV9-PLA2G4E, and compared to that in the sham-injected group. Administration of the virus provoked a marked increase in PLA2G4E mRNA and protein expression compared to the sham-injected animals (Supplementary Fig.S9A, B). To determine the mechanisms underlying memory improvement, both pathological amyloid and tau, as well as dendritic synaptic density, were analysed. Mice overexpressing PLA2G4E had similar levels of soluble $A\beta_{42}$ ($t=0.2538$, $P=0.8036$: Fig. 7D) and ptau ($F(2,11)=1.010$,

P=0.3955, one way ANOVA: Figure 7E) to the sham-injected mice, yet they had significant more dendritic spines (one way ANOVA effect of group $F(2,98)=4.985$, $P<0.001$: Fig. 7F), consistent with the cognitive improvement observed. These results are reported in the patent No 19382563.5 (Cuadrado-Tejedor et al., 2019).

4. Discussion

In this study, a widely used mouse model of AD (Tg2576) and human samples have been used to demonstrate that stronger expression of neuronal PLA2G4E promotes cognitive resilience to pathological AD. We identified a novel 13 bp deletion in the promoter region of Pla2g4E that was more prevalent in the resilient mice and that may be responsible for the stronger Pla2g4E expression in these mice. Indeed, in a different AD mouse model (APP/PS1) AAV–mediated hippocampal expression of PLA2G4E reverses the cognitive deficits in these mice. The amelioration of memory deficits was correlated with an increase in synaptic density, without affecting the pathological amyloid or tau, further suggesting that PLA2G4E is involved in the molecular mechanisms underlying resilience. Furthermore, we demonstrate for the first time that PLA2G4E is down-regulated in severe AD conditions, both in animal models and humans. Overall, our study highlights the potential of PLA2G4E overexpression as a novel therapeutic strategy for AD and for other diseases that course with memory impairment.

In accordance with several longitudinal studies showing that amyloid plaques and NFTs are not limited to individuals with dementia (Crystal et al., 1988; Dickson et al., 1992; Hulette et al., 1998; Katzman et al., 1988; Knopman et al., 2003; Price et al., 1991; Schmitt et al., 2000; Tomlinson et al., 1968), we demonstrate the existence of asymptomatic resilient individuals (about 22%) in the Tg2576 model of AD. A similar finding was previously reported in the 5xFAD model, where 30% of 8 mo mice displayed intact memory in the FC test (Neuner et al., 2017). In fact, individuals that escape from the expected severe phenotype have been also identified in other animal disease models (Zucconi et al., 2010). A careful and in depth comparison of these individuals with those experiencing disease symptoms could help identify new potential therapeutic targets. Indeed, animal models provide a powerful tool to avoid genetic diversity, medication or different environmental factors that can bias conventional longitudinal studies carried out in humans. Animal models also provide a powerful

resource to analyze the transcriptome, since RNA integrity is crucial to study gene expression and such studies in the human brain relies on post-mortem tissue, associated with poorer (and variable) RNA integrity, which may affect gene expression. Thus, identifying the molecular basis enabling "resilient" animals to retain normal cognition despite the presence of pathological elements associated with AD could lead to more targeted AD treatments. Accordingly, PLA2G4E was identified in transcriptome analyses as potentially contributing to resistance against dementia in aged Tg2576 mice. A 13 bp deletion in the regulatory region of Pla2g4E predicts the presence of a binding site for the SP1 transcriptional activator, which may modulate its expression and contribute to its resilience in Tg2576 mice. However, further experiments will be necessary to demonstrate the presence of a functional SP1 responsive element in the Pla2g4E promoter of resilient mice.

To confirm the validity of this finding, PLA2G4E expression was analyzed in human brain samples from AD patients and healthy individuals. Accordingly, PLA2G4E was downregulated in AD subjects at late stages of the disease and with dementia, while at early stages of AD, when no cognitive impairment was reported, PLA2G4E at the time of death remained at the same levels as the controls. Thus, the loss of PLA2G4E might play a key role in AD progression and specifically, in the onset of dementia. To understand the influence of PLA2G4E in AD progression and its role in maintaining synaptic function, it will be interesting to assess whether "cognitive resilient" or asymptomatic patients with similar neuropathological AD hallmarks as classical AD patients maintain enhanced PLA2G4E expression in the brain. As we found in Tg2576 mice (Fig. 4), it is possible that also in humans specific genetic variants could be responsible for decreasing or increasing PLA2G4E expression, thereby altering the risk of developing AD associated dementia. Interestingly, GWAS identified a PLA2G4E gene variant associated with altered CSF APOE protein levels: rs12232304 (Cruchaga et al., 2012). Similar genetic studies focused on identifying genetic variants associated with soluble CSF TREM2 also revealed a different PLA2G4E gene variant: rs7182355 (Piccio et al., 2016).

PLA2G4E is a poorly characterized cytosolic PLA2 phospholipase that is expressed strongly in the brain, heart, testis and skeletal muscle of mice (Ogura et al., 2016). To unravel the specific role of PLA2G4E in cognitive resilience and AD pathogenesis, its distribution in the brain was characterized. Apart from confirming its neural and

cytosolic location (Ogura et al., 2016), we demonstrate that PLA2G4E is also present in the dendrites of pyramidal cells and in the extrasynaptic plasma membrane. The neuronal location of PLA2G4E at the synapse, together with its up-regulation in the brain of cognitively resilient subjects suggests that this enzyme may play a role in memory. To obtain more direct evidence for the role of PLA2G4E in learning and memory, we assessed whether PLA2G4E expression was regulated by the FC test, which requires hippocampal-dependent transcription and protein synthesis. Interestingly, we found that PLA2G4E expression increased in the hippocampus and cortex during memory retrieval, suggesting that PLA2G4E is involved in memory. Furthermore, we demonstrated that in primary neurons, where NMDA receptors activation was induced by bicuculline, AAV-PLA2G4E-shRNA effectively blocked the activation of different neural plasticity genes such as CREB, GluA1 and synapsin I. These experiments indicate that synaptic activity seems to be altered upon PLA2G4E knockdown. Thus, although specific electrophysiological studies should be conducted to further demonstrate the specific role of PLA2G4E in neural transmission, these data points PLA2G4E as one of the players of NMDA receptor activation.

Taken together these data and the fact that the overexpression of PLA2G4E in aged-APP/PS1 mice completely reversed spatial memory deficits, we could hypothesize that PLA2G4E overexpression may be a useful therapeutic strategy to combat signs of dementia in the context of AD.

The mechanism underlying the cognitive improvement associated with PLA2G4E expression may involve an increase in the number of dendritic spines, which is independent of the pathological changes in amyloid and tau. The results obtained are in agreement with earlier data whereby the treatment with phosphatidylserine, a phospholipid that activates PLA2G4E (Binte Mustafiz et al., 2019), improved memory deficits in AD rats and patients (Zhang et al., 2015).. Moreover, PLA2G4E was recently described as the calcium-dependent N-acyltransferase that produces N-acyl phosphatidylethanolamines (NAPEs), precursors of N-acyl ethanolamine (NAE) and lipid transmitters like the endocannabinoid anandamide (Ogura et al., 2016). Maroof et al. described a reduction in the endocannabinoids anandamide and 2-arachidonoyl glycerol in the striatum of 8-month-old APP/PS1 mice that may contribute to the cognitive impairments observed in these mice (Maroof et al., 2014). Consequently, the

restoration of memory deficits following PLA2G4E overexpression may be caused, at least in part, by enhancing these endocannabinoids.

PLA2G4E co-localizes with the ADP-ribosylation factor 6 (ARF6) at the surface of the early clathrin-independent endosomes of transfected HeLa cells (Capestrano et al., 2014), with ARF6 specifically implicated in the endocytosis of plasma membrane proteins and to a lesser extent, with plasma membrane protein recycling. Interestingly, ARF6 has been reported to play a role in neurite outgrowth (Cheung et al., 2014; Hernández-Deviez et al., 2004)and dendritic spine maturation(Kim et al., 2015)), although its function in mature synapses is largely unknown. It is possible that PLA2G4E and ARF6 also co-localize in neurons, performing a similar function and thereby contributing to synaptic plasticity, although further experiments will be necessary to prove this.

In summary, for the first time we demonstrate here a link between PLA2G4E up-regulation and the ability to cope with the pathological changes associated with AD, without developing dementia. These findings suggest that PLA2G4E may be a novel target to manage AD, as well as other diseases that course with cognitive impairment.

6. Funding

We gratefully acknowledge grant support from Health department of Gobierno de Navarra with exp. 67/2017, 50% co-financed by the European Regional Development Fund through the 2014 ERDF Operational Program-2020, as well as to the Foundation for Applied Medical Research, the University of Navarra (Pamplona, Spain) for financial support and the Asociación de Amigos of the University of Navarra for the grant to MPG and SB.

7. Competing interests

The authors report no competing interests. The Patent. No 19382563.5., cPLA2e INDUCING AGENTS AND USES THEREOF, relates to the results present in the paper.

5. Acknowledgements

We thank Dr Ivan Martinez-Valbuena and Nerea Juanarena for their intellectual discussion and technical assistance. And also Prof. Marina Lynch for having accepted MPG for an internship in her laboratory.

8. References

Aerts, S., Thijs, G., Coessens, B., Staes, M., Moreau, Y., De Moor, B., 2003. Toucan: Deciphering the cis-regulatory logic of coregulated genes. Nucleic Acids Res. https://doi.org/10.1093/nar/gkg268

Arnold, F.J.L., Hoffmann, F., Bengtson, C.P., Wittmann, M., Vanhoutte, P., Bading, H., 2005. Microelectrode array recordings of cultured hippocampal networks reveal a simple model for transcription and protein synthesis-dependent plasticity. J. Physiol. 564, 3–19. https://doi.org/10.1113/jphysiol.2004.077446

Barroeta-Espar, I., Weinstock, L.D., Perez-Nievas, B.G., Meltzer, A.C., Siao Tick Chong, M., Amaral, A.C., Murray, M.E., Moulder, K.L., Morris, J.C., Cairns, N.J., Parisi, J.E., Lowe, V.J., Petersen, R.C., Kofler, J., Ikonomovic, M.D., López, O., Klunk, W.E., Mayeux, R.P., Frosch, M.P., Wood, L.B., Gomez-Isla, T., 2019. Distinct cytokine profiles in human brains resilient to Alzheimer's pathology. Neurobiol. Dis. 121, 327–337. https://doi.org/10.1016/j.nbd.2018.10.009

Bennett, D.A., Wilson, R.S., Boyle, P.A., Buchman, A.S., Schneider, J.A., 2012. Relation of neuropathology to cognition in persons without cognitive impairment. Ann. Neurol. 72, 599–609. https://doi.org/10.1002/ana.23654

Binte Mustafiz, S.S., Uyama, T., Hussain, Z., Kawai, K., Tsuboi, K., Araki, N., Ueda, N., 2019. The role of intracellular anionic phospholipids in the production of N-acyl-phosphatidylethanolamines by cytosolic phospholipase A2ε. J. Biochem. 165, 343–352. https://doi.org/10.1093/jb/mvy104

Brumback-Peltz, C., Balasubramanian, A.B., Corrada, M.M., Kawas, C.H., 2011. Diagnosing dementia in the oldest-old. Maturitas 70, 164–8. https://doi.org/10.1016/j.maturitas.2011.07.008

Bullain, S.S., Corrada, M.M., Shah, B.A., Mozaffar, F.H., Panzenboeck, M., Kawas,

C.H., 2013. Poor physical performance and dementia in the oldest old: The 90+ study. Arch. Neurol. 70, 107–113. https://doi.org/10.1001/jamaneurol.2013.583

Capestrano, M., Mariggio, S., Perinetti, G., Egorova, A. V, Iacobacci, S., Santoro, M., Di Pentima, A., Iurisci, C., Egorov, M. V, Di Tullio, G., Buccione, R., Luini, A., Polishchuk, R.S., 2014. Cytosolic phospholipase A_2 ε drives recycling through the clathrin-independent endocytic route. J. Cell Sci. 127, 977–93. https://doi.org/10.1242/jcs.136598

Caspers, S., Moebus, S., Lux, S., Pundt, N., Schütz, H., Mühleisen, T.W., Gras, V., Eickhoff, S.B., Romanzetti, S., Stöcker, T., Stirnberg, R., Kirlangic, M.E., Minnerop, M., Pieperhoff, P., Mödder, U., Das, S., Evans, A.C., Jöckel, K.-H., Erbel, R., Cichon, S., Nöthen, M.M., Sturma, D., Bauer, A., Jon Shah, N., Zilles, K., Amunts, K., 2014. Studying variability in human brain aging in a population-based German cohort-rationale and design of 1000BRAINS. Front. Aging Neurosci. 6, 149. https://doi.org/10.3389/fnagi.2014.00149

Cesca, F., Baldelli, P., Valtorta, F., Benfenati, F., 2010. The synapsins: key actors of synapse function and plasticity. Prog. Neurobiol. 91, 313–48. https://doi.org/10.1016/j.pneurobio.2010.04.006

Cheung, H.N.M., Dunbar, C., Mórotz, G.M., Cheng, W.H., Chan, H.Y.E., Miller, C.C.J., Lau, K.-F., 2014. FE65 interacts with ADP-ribosylation factor 6 to promote neurite outgrowth. FASEB J. 28, 337–49. https://doi.org/10.1096/fj.13-232694

Cruchaga, C., Kauwe, J.S.K., Nowotny, P., Bales, K., Pickering, E.H., Mayo, K., Bertelsen, S., Hinrichs, A., Fagan, A.M., Holtzman, D.M., Morris, J.C., Goate, A.M., 2012. Cerebrospinal fluid APOE levels: An endophenotype for genetic studies for Alzheimer's disease. Hum. Mol. Genet. 21, 4558–4571. https://doi.org/10.1093/hmg/dds296

Durocher, Y., Perret, S., Kamen, A., 2002. High-level and high-throughput recombinant protein production by transient transfection of suspension-growing human 293-EBNA1 cells. Nucleic Acids Res. 30, 9e – 9. https://doi.org/10.1093/nar/30.2.e9

Ewbank, D.C., Arnold, S.E., 2009. Cool with Plaques and Tangles. N. Engl. J. Med. 360, 2357–2359. https://doi.org/10.1056/NEJMe0901965

Ferrer, I., Martinez, A., Boluda, S., Parchi, P., Barrachina, M., 2008. Brain banks: benefits, limitations and cautions concerning the use of post-mortem brain tissue for molecular studies. Cell Tissue Bank. 9, 181–94. https://doi.org/10.1007/s10561-008-9077-0

Giese, K.P., Mizuno, K., 2013. The roles of protein kinases in learning and memory. Learn. Mem. https://doi.org/10.1101/lm.028449.112

Ginty, D.D., Kornhauser, J.M., Thompson, M.A., Bading, H., Mayo, K.E., Takahashi, J.S., Greenberg, M.E., 1993. Regulation of CREB phosphorylation in the suprachiasmatic nucleus by light and a circadian clock. Science (80-.). 260, 238–241. https://doi.org/10.1126/science.8097062

Glaser, E.M., Van der Loos, H., 1981. Analysis of thick brain sections by obverse—Reverse computer microscopy: Application of a new, high clarity Golgi—Nissl stain. J. Neurosci. Methods 4, 117–125.

Guntupalli, S., Widagdo, J., Anggono, V., 2016. Amyloid-β-Induced Dysregulation of AMPA Receptor Trafficking. Neural Plast. 2016, 3204519. https://doi.org/10.1155/2016/3204519

Hardingham, G.E., Fukunaga, Y., Bading, H., 2002. Extrasynaptic NMDARs oppose synaptic NMDARs by triggering CREB shut-off and cell death pathways. Nat. Neurosci. 5, 405–414. https://doi.org/10.1038/nn835

Haroutunian, V., Schnaider-Beeri, M., Schmeidler, J., Wysocki, M., Purohit, D.P., Perl, D.P., Libow, L.S., Lesser, G.T., Maroukian, M., Grossman, H.T., 2008. Role of the neuropathology of Alzheimer disease in dementia in the oldest-old. Arch. Neurol. 65, 1211–1217. https://doi.org/10.1001/archneur.65.9.1211

Hernández-Deviez, D.J., Roth, M.G., Casanova, J.E., Wilson, J.M., 2004. ARNO and ARF6 regulate axonal elongation and branching through downstream activation of phosphatidylinositol 4-phosphate 5-kinase alpha. Mol. Biol. Cell 15, 111–20. https://doi.org/10.1091/mbc.e03-06-0410

Hill, J.T., Demarest, B.L., Bisgrove, B.W., Su, Y.C., Smith, M., Yost, H.J., 2014. Poly peak parser: Method and software for identification of unknown indels using sanger sequencing of polymerase chain reaction products. Dev. Dyn. 243, 1632–

1636. https://doi.org/10.1002/dvdy.24183

Hsiao, K., Chapman, P., Nilsen, S., Eckman, C., Harigaya, Y., Younkin, S., Yang, F., Cole, G., 1996. Correlative Memory Deficits, Aβ Elevation, and Amyloid Plaques in Transgenic Mice. Science (80-.). 274, 99–103.

Huff, N.C., Frank, M., Wright-Hardesty, K., Sprunger, D., Matus-Amat, P., Higgins, E., Rudy, J.W., 2006. Amygdala regulation of immediate-early gene expression in the hippocampus induced by contextual fear conditioning. J. Neurosci. 26, 1616–1623. https://doi.org/10.1523/JNEUROSCI.4964-05.2006

Iacono, D., Markesbery, W.R., Gross, M., Pletnikova, O., Rudow, G., Zandi, P., Troncoso, J.C., 2009. The Nun Study: Clinically silent AD, neuronal hypertrophy, and linguistic skills in early life. Neurology 73, 665–673. https://doi.org/10.1212/WNL.0b013e3181b01077

Iacono, D., O'Brien, R., Resnick, S.M., Zonderman, A.B., Pletnikova, O., Rudow, G., An, Y., West, M.J., Crain, B., Troncoso, J.C., 2008. Neuronal Hypertrophy in Asymptomatic Alzheimer Disease. J. Neuropathol. Exp. Neurol. 67, 578–589. https://doi.org/10.1097/NEN.0b013e3181772794

Irizarry, R.A., Bolstad, B.M., Collin, F., Cope, L.M., Hobbs, B., Speed, T.P., 2003. Summaries of Affymetrix GeneChip probe level data. Nucleic Acids Res. 31, e15.

Kida, S., Josselyn, S.A., De Ortiz, S.P., Kogan, J.H., Chevere, I., Masushige, S., Silva, A.J., 2002. CREB required for the stability of new and reactivated fear memories. Nat. Neurosci. 5, 348–355. https://doi.org/10.1038/nn819

Kim, Y., Lee, S.E., Park, J., Kim, M., Lee, B., Hwang, D., Chang, S., 2015. ADP-ribosylation factor 6 (ARF6) bidirectionally regulates dendritic spine formation depending on neuronal maturation and activity. J. Biol. Chem. 290, 7323–7335. https://doi.org/10.1074/jbc.M114.634527

Lace, G., Savva, G.M., Forster, G., de Silva, R., Brayne, C., Matthews, F.E., Barclay, J.J., Dakin, L., Ince, P.G., Wharton, S.B., MRC-CFAS, 2009. Hippocampal tau pathology is related to neuroanatomical connections: an ageing population-based study. Brain 132, 1324–1334. https://doi.org/10.1093/brain/awp059

Livak, K.J., Schmittgen, T.D., 2001. Analysis of relative gene expression data using real-time quantitative PCR and the 2(-Delta Delta C(T)) Method. Methods 25, 402–408. https://doi.org/10.1006/meth.2001.1262

Luján, R., Shigemoto, R., 2006. Localization of metabotropic GABA receptor subunits GABA $_{B1}$ and GABA $_{B2}$ relative to synaptic sites in the rat developing cerebellum. Eur. J. Neurosci. 23, 1479–1490. https://doi.org/10.1111/j.1460-9568.2006.04669.x

Maroof, N., Ravipati, S., Pardon, M.C., Barrett, D.A., Kendalla, D.A., 2014. Reductions in Endocannabinoid Levels and Enhanced Coupling of Cannabinoid Receptors in the Striatum are Accompanied by Cognitive Impairments in the AβPPswe/PS1ΔE9 Mouse Model of Alzheimer's Disease. J. Alzheimer's Dis. 42, 227–245. https://doi.org/10.3233/JAD-131961

Megías, M., Emri, Z., Freund, T.F., Gulyás, A.I., 2001. Total number and distribution of inhibitory and excitatory synapses on hippocampal CA1 pyramidal cells. Neuroscience 102, 527–40.

Negash, S., Wilson, R., Leurgans, S., Wolk, D., Schneider, J., Buchman, A., Bennett, D., Arnold, S., 2013. Resilient Brain Aging: Characterization of Discordance between Alzheimer's Disease Pathology and Cognition. Curr. Alzheimer Res. 10, 844–851. https://doi.org/10.2174/15672050113109990157

Neuner, S.M., Wilmott, L.A., Hoffmann, B.R., Mozhui, K., Kaczorowski, C.C., 2017. Hippocampal proteomics defines pathways associated with memory decline and resilience in normal aging and Alzheimer's disease mouse models. Behav. Brain Res. 322, 288–298. https://doi.org/10.1016/j.bbr.2016.06.002

O'Brien, R.J., Resnick, S.M., Zonderman, A.B., Ferrucci, L., Crain, B.J., Pletnikova, O., Rudow, G., Iacono, D., Riudavets, M.A., Driscoll, I., Price, D.L., Martin, L.J., Troncoso, J.C., 2009. Neuropathologic Studies of the Baltimore Longitudinal Study of Aging (BLSA). J. Alzheimer's Dis. 18, 665–675. https://doi.org/10.3233/JAD-2009-1179

Ogura, Y., Parsons, W.H., Kamat, S.S., Cravatt, B.F., 2016. A calcium-dependent acyltransferase that produces N-acyl phosphatidylethanolamines. Nat. Chem. Biol.

12, 669–671. https://doi.org/10.1038/nchembio.2127

Perez-Nievas, B.G., Stein, T.D., Tai, H.-C., Dols-Icardo, O., Scotton, T.C., Barroeta-Espar, I., Fernandez-Carballo, L., de Munain, E.L., Perez, J., Marquie, M., Serrano-Pozo, A., Frosch, M.P., Lowe, V., Parisi, J.E., Petersen, R.C., Ikonomovic, M.D., López, O.L., Klunk, W., Hyman, B.T., Gómez-Isla, T., 2013. Dissecting phenotypic traits linked to human resilience to Alzheimer's pathology. Brain 136, 2510–2526. https://doi.org/10.1093/brain/awt171

Piccio, L., Deming, Y., Del-Águila, J.L., Ghezzi, L., Holtzman, D.M., Fagan, A.M., Fenoglio, C., Galimberti, D., Borroni, B., Cruchaga, C., 2016. Cerebrospinal fluid soluble TREM2 is higher in Alzheimer disease and associated with mutation status. Acta Neuropathol. 131, 925–933. https://doi.org/10.1007/s00401-016-1533-5

Porte, Y., Buhot, M.-C., Mons, N., 2008a. Alteration of CREB phosphorylation and spatial memory deficits in aged 129T2/Sv mice. Neurobiol. Aging 29, 1533–46. https://doi.org/10.1016/j.neurobiolaging.2007.03.023

Porte, Y., Buhot, M.C., Mons, N.E., 2008b. Spatial memory in the Morris water maze and activation of cyclic AMP response element-binding (CREB) protein within the mouse hippocampus. Learn. Mem. 15, 885–894. https://doi.org/10.1101/lm.1094208

Puig, B., Gómez-Isla, T., Ribé, E., Cuadrado, M., Torrejón-Escribano, B., Dalfó, E., Ferrer, I., 2004. Expression of stress-activated kinases c-Jun N-terminal kinase (SAPK/JNK-P) and p38 kinase (p38-P), and tau hyperphosphorylation in neurites surrounding betaA plaques in APP Tg2576 mice. Neuropathol. Appl. Neurobiol. 30, 491–502. https://doi.org/10.1111/j.1365-2990.2004.00569.x

Rao, V.R., Pintchovski, S.A., Chin, J., Peebles, C.L., Mitra, S., Finkbeiner, S., 2006. AMPA receptors regulate transcription of the plasticity-related immediate-early gene Arc. Nat. Neurosci. 9, 887–95. https://doi.org/10.1038/nn1708

Sato, K., Morimoto, K., Suemaru, S., Sato, T., Yamada, N., 2000. Increased synapsin I immunoreactivity during long-term potentiation in rat hippocampus. Brain Res. 872, 219–22. https://doi.org/10.1016/s0006-8993(00)02460-4

Savva GM; Wharton SB; Ince PG; Forster G; Matthews FE; Brayne C; Medical Research Council Cognitive Function and Ageing, 2009. Age, neuropathology, and dementia. N Engl J Med. 360, 2302–2309.

Serneels L, Van Biervliet J, Craessaerts K, Dejaegere T, Horré K, Van Houtvin T, D.S.B., 2009. γ-Secretase heterogeneity in the Aph1 subunit: relevance for Alzheimer's disease. Science (80-.). 324, 639–642.

Serrano-Pozo, A., Frosch, M.P., Masliah, E., Hyman, B.T., 2011. Neuropathological Alterations in Alzheimer Disease. Cold Spring Harb. Perspect. Med. 1, a006189–a006189. https://doi.org/10.1101/cshperspect.a006189

Shlisky, J., Bloom, D.E., Beaudreault, A.R., Tucker, K.L., Keller, H.H., Freund-Levi, Y., Fielding, R.A., Cheng, F.W., Jensen, G.L., Wu, D., Meydani, S.N., 2017. Nutritional Considerations for Healthy Aging and Reduction in Age-Related Chronic Disease. Adv. Nutr. An Int. Rev. J. 8, 17.2-26. https://doi.org/10.3945/an.116.013474

Smyth, G.K., 2004. Linear models and empirical bayes methods for assessing differential expression in microarray experiments. Stat. Appl. Genet. Mol. Biol. 3, Article3. https://doi.org/10.2202/1544-6115.1027

Stern, Y., 2012. Cognitive reserve in ageing and Alzheimer's disease. Lancet Neurol. 11, 1006–1012. https://doi.org/10.1016/S1474-4422(12)70191-6

Tomlinson, B.E., Blessed, G., Roth, M., 1968. Observations on the brains of non-demented old people. J. Neurol. Sci. 7, 331–356. https://doi.org/10.1016/0022-510X(68)90154-8

Tyas, S.L., Snowdon, D.A., Desrosiers, M.F., Riley, K.P., Markesbery, W.R., 2007. Healthy ageing in the Nun Study: definition and neuropathologic correlates. Age Ageing 36, 650–655. https://doi.org/10.1093/ageing/afm120

Untergasser, A., Cutcutache, I., Koressaar, T., Ye, J., Faircloth, B.C., Remm, M., Rozen, S.G., 2012. Primer3-new capabilities and interfaces. Nucleic Acids Res. 40. https://doi.org/10.1093/nar/gks596

Vieira, N.M., Elvers, I., Alexander, M.S., Moreira, Y.B., Eran, A., Gomes, J.P.,

Marshall, J.L., Karlsson, E.K., Verjovski-Almeida, S., Lindblad-Toh, K., Kunkel, L.M., Zatz, M., 2015. Jagged 1 Rescues the Duchenne Muscular Dystrophy Phenotype. Cell 163, 1204–1213. https://doi.org/10.1016/j.cell.2015.10.049

Westerman, M.A., Cooper-Blacketer, D., Mariash, A., Kotilinek, L., Kawarabayashi, T., Younkin, L.H., Carlson, G.A., Younkin, S.G., Ashe, K.H., 2002. The relationship between Aβ and memory in the Tg2576 mouse model of Alzheimer's disease. J. Neurosci. 22, 1858–1867. https://doi.org/10.1523/jneurosci.22-05-01858.2002

White, L., 2009. Brain Lesions at Autopsy in Older Japanese-American Men as Related to Cognitive Impairment and Dementia in the Final Years of Life: A Summary Report from the Honolulu-Asia Aging Study. J. Alzheimer's Dis. 18, 713–725. https://doi.org/10.3233/JAD-2009-1178

Zhang, Y.Y., Yang, L.Q., Guo, L.M., 2015. Effect of phosphatidylserine on memory in patients and rats with Alzheimer's disease. Genet. Mol. Res. 14, 9325–9333. https://doi.org/10.4238/2015.August.10.13

Zolotukhin, S., Byrne, B.J., Mason, E., Zolotukhin, I., Potter, M., Chesnut, K., Summerford, C., Samulski, R.J., Muzyczka, N., 1999. Recombinant adeno-associated virus purification using novel methods improves infectious titer and yield. Gene Ther. 6, 973–985. https://doi.org/10.1038/sj.gt.3300938

Zucconi, E., Valadares, M.C., Vieira, N.M., Bueno, C.R., Secco, M., Jazedje, T., Almeida da Silva, H.C., Vainzof, M., Zatz, M., 2010. Ringo: Discordance between the molecular and clinical manifestation in a Golden Retriever Muscular Dystrophy dog. Neuromuscul. Disord. 20, 64–70. https://doi.org/10.1016/j.nmd.2009.10.011

Figure Legends

Fig. 1. Identification of Tg2576 cognitive resilient mice through MWM test. (A) Escape latency of the visible-platform phase in the MWM test for WT and Tg2576

mice, indicating that all the selected mice were able to perform the task in the same conditions. (B) Escape latency to the hidden-platform in the MWM test for WT and Tg2576 mice, confirming the spatial memory deficit characteristic of aged-Tg2576 mice (Two way ANOVA test followed by Bonferroni's post hoc test, n=18-22, ***P≤0.001). (C) Escape latency to the hidden-platform in the reversal MWM test performed two months later for WT, Imp_Tg2576 and Res_Tg2576 mice showing that similarly to WT mice, Res_Tg2576 mice do not present spatial memory impairment (Two way ANOVA test followed by Bonferroni's post hoc test, n=4-5, **P≤0.01 WT versus Imp_Tg2576, ***P≤0.001 WT versus Imp_Tg2576, $$$P≤0.001 WT versus Res_Tg2576, +P≤0.05 Imp_Tg2576 versus Res_Tg2576, +++P≤0.001 Imp_Tg2576 versus Res_Tg2576). (D) Percentage of time spent in the correct quadrant during the probe trial on day 5th, supporting the fact that Res_Tg2576 mice maintain intact spatial memory retention (One way ANOVA test followed by Newman-Kewls post hoc test, n=4-5, ***P≤0.001 WT versus Imp_Tg2576, $P≤0.05 WT versus Res_Tg2576, +++P≤0.001 Imp_Tg2576 versus Res_Tg2576).

Fig. 2. An increased expression of synaptic markers is observed in aged-Tg2576 cognitive resilient mice despite evidence of amyloid burden, tau pathology and augmented neuroinflammation. (A) Soluble Aβ42 levels in parieto-temporal cortical extracts measured by ELISA. (B) ptau and (C) pGSK3β levels analysed by immunoblotting in pre-frontal cortex extracts and normalized vs β-actin (One way ANOVA test followed by Newman-Kewls post hoc test, n=4-5, **P≤0.01 WT versus Imp_Tg2576, $$P≤0.01 WT versus Res_Tg2576). (D) Hippocampal mRNA levels of the neuroinflammatory markers GFAP and CD11b detected by qRT-PCR (One way ANOVA test followed by Newman-Kewls post hoc test, n=4-5, **P≤0.01 WT versus Imp_Tg2576, $P≤0.05 WT versus Res_Tg2576). (E) Pre-frontal cortex pCREB and synapsin I levels measured by immunoblotting and normalized vs β-actin (One way ANOVA test followed by Newman-Kewls post hoc test, n=4-5, $$P≤0.01 WT versus Res_Tg2576, +P≤0.05 Imp_Tg2576 versus Res_Tg2576, ++P≤0.01 Imp_Tg2576 versus Res_Tg2576). (F) Levels of the synaptic markers PSD95, synaptophysin, pCAMKII, GluN2B and pGluA1 analysed in prefrontal cortex extracts by immunoblotting (One way ANOVA test followed by Newman-Keuls post hoc test, n=4-5, ***P≤0.001 WT versus Imp_Tg2576, $P≤0.05 WT versus Res_Tg2576, $$$P≤0.001 WT versus

Res_Tg2576). Data are expressed as arbitrary units (mean ± SEM) with respect to their respective controls.

Fig. 3. PLA2G4E is involved both in cognitive resilience and AD pathophysiology. (A) Relative hippocampal PLA2G4E mRNA expression analysed by RT-PCR and normalized with 36B4 in WT, Imp_Tg2576 and Res_Tg2576 (unpaired two-tailed Student's t-test, n=4, +P≤0.05 Imp_Tg2576 versus Res_Tg2576) (B) Parieto-temporal cortex PLA2G4E levels assayed by immunoblotting and normalized with β-actin in WT, Imp_Tg2576 and Res_Tg2576 (n=4-5). (C) PLA2G4E and (D) synapsin I levels from control (n=8), II-IV Braak AD (n=10) and V-VI Braak AD (n=9) individuals measured by immunoblotting in temporal extracts and normalized vs β-actin (one-way ANOVA test followed by Newman-Keuls post hoc test, n=8-10, *P≤0.05 control versus V-VI Braak AD, +P≤0.05 II-IV Braak vs V-VI Braak).

Fig. 4. **A 13-bp deletion allele in Pla2g4E promoter is associated with resilience**. (A) The upper panel depicts a genomic map of the 5'UTR region of the Pla2g4E gene as shown by USCS Genome Browser GRCm38/mm10 mouse assembly. The 427-bp amplicon screened for genomic variants is represented by a horizontal black bar below the map gene. Yellow bar corresponds to the location of rs226296356 (dbSNP v142) polymorphism. The square below shows a zoomed-in view of the genomic region harboring 13-bp deletion (represented as a thin line with arrows within the 427-bp amplicon). All dbSNP v142 polymorphisms are displayed below the amplicon; single nucleotide variations in blue and indel variations in red. Repeating elements are shown as horizontal black box below polymorphisms. Vertical arrows point to rs45716056 (red) and rs265703496 (blue) which are also depicted in panel B. (B) Electropherogram examples of 13-bp indel genotyping are shown in panel B. Vertical blue line indicates the genomic position where 13-bp indel starts. Horizontal grey bar overlaps the 13 deleted base pairs. Reference genomic sequence is represented in the upper line. Vertical red arrow points to rs45716056 (G/T) and blue arrow indicates rs265703496 (A/G). (C) Stacked bar chart represents differential distribution of 13-bp deletion allele between resilient and non-resilient mice (p-value ≤ 0.05).

Fig. 5. Within the brain, PLA2G4E is expressed in the neurons where it mainly has a cytosolic location although it is also present in the dendrites and dendritic spines. (A) Immunofluorescence assay showing colocalization of PLA2G4E and MAP2 in

murine primary neuronal cultures at day in vitro (DIV) 14. (B) Hippocampal paraffin-embedded human sections immunostained with PLA2G4E anti-serum and counterstained with hematoxylin–eosin. Scale bar=20μm. (C) Subsynaptic distribution of PLA2G4E in the CA1 region of mice hippocampi using pre-embedding immunogold technique. Den: dendrite (Den); s: dendritic spines; at: axon terminals. Arrows indicates extrasynaptic plasma membrane location and crossed arrows intracellular sites in dendritic spines. Scale bar = 500 nm.

Fig. 6. PLA2G4E plays a role in memory function, specifically in the process of memory retrieval. (A) Diagram showing the experimental design of the Fear Conditioning paradigm used to elucidate the role of PLA2G4E in memory function. Graph indicating the percentage of freezing behaviour of TT mice during the training and test phase respectively (B) pCREB and (C) PLA2G4E levels measured by immunoblotting in hippocampal extracts and normalized vs β-actin (one-way ANOVA test followed by Newman-Kewls post hoc test, n=7-8, **P≤0.01 Naïve vs TT, ++P≤0.01 T24 vs TT). (D) The knockdown of PLA2G4E blocks the activation of synaptic proteins involved in synaptic transmission. Levels of pCREB, pGluA1, synapsin I and PLA2G4E levels were measured by immunoblotting and normalized vs β-actin in primary neuronal cultures after treatment with bicuculline (Bic) and/or AAV9-PLA2G4E-shRNA (shPLA) (One way ANOVA test followed by Newman-Kewls post hoc test, n=3-6, **P≤0.01, ***P≤0.001 control versus Bic; ++P≤0.01 control vs shPLA; $P≤0.05, $$P≤0.01, $$$P≤0.001 Bic versus shPLA+Bic). Data are expressed as arbitrary units (mean ± SEM) with respect to controls.

Fig. 7. Hippocampal PLA2G4E overexpression completely reverses cognitive impairment in aged-APP/PS1 mice by increasing dendritic spine density and without affecting amyloid and tau pathology. (A) Escape latency of the visible-platform phase for WT, APP/PS1 sham and APP/PS1 AAV9_PLA2G4E mice (two-way ANOVA test followed by Bonferroni's post hoc test, n=6-9, **P≤0.01 WT vs APP/PS1 sham, ++P≤0.01 WT vs APP/PS1 AAV9_PLA2G4E). (B) Escape latency to the hidden-platform phase for WT, APP/PS1 sham and APP/PS1 AAV9_PLA2G4E mice (two-way ANOVA test followed by Bonferroni's post hoc test, n=6-9, *P≤0.05 WT vs APP/PS1 sham, **P≤0.01 WT vs APP/PS1 sham, +P≤0.05 WT vs APP/PS1 AAV9_PLA2G4E, $P≤0.05 APP/PS1 sham versus APP/PS1 AAV9_PLA2G4E, $$P≤0.01 APP/PS1 sham versus APP/PS1 AAV2/9_PLA2G4E). (C) Percentage of time spent in the correct

quadrant during the probe trial on days 6th and 8th performed by for WT, APP/PS1 sham and APP/PS1 AAV9_PLA2G4E mice (One way ANOVA test followed by Newman-Kewls post hoc test, n=6-9, *P≤0.05 WT versus APP/PS1 sham, **P≤0.01 WT versus APP/PS1 sham). D) Soluble Aβ42 levels in SDS 2% hippocampal samples from elderly APP/PS1 sham or AAV9_PLA2G4E injected mice measured by ELISA (n=6-9). E) ptau levels analyzed by immunoblotting in hippocampal SDS extracts and normalized vs β-actin. F) Representative Golgi staining images of apical dendrites on CA1 hippocampal pyramidal neurons (Scale bar=10 µm) and histoblot showing spine density quantification of those neurons in WT, APP/PS1 sham and AAV9_PLA2G4E treated mice (one-way ANOVA test followed by Newman-Kewls post hoc test, n=4, +P≤0.05 WT vs APP/PS1 AAV9_PLA2G4E, $P ≤0.05 APP/PS1 sham versus APP/PS1 AAV9_PLA2G4E).

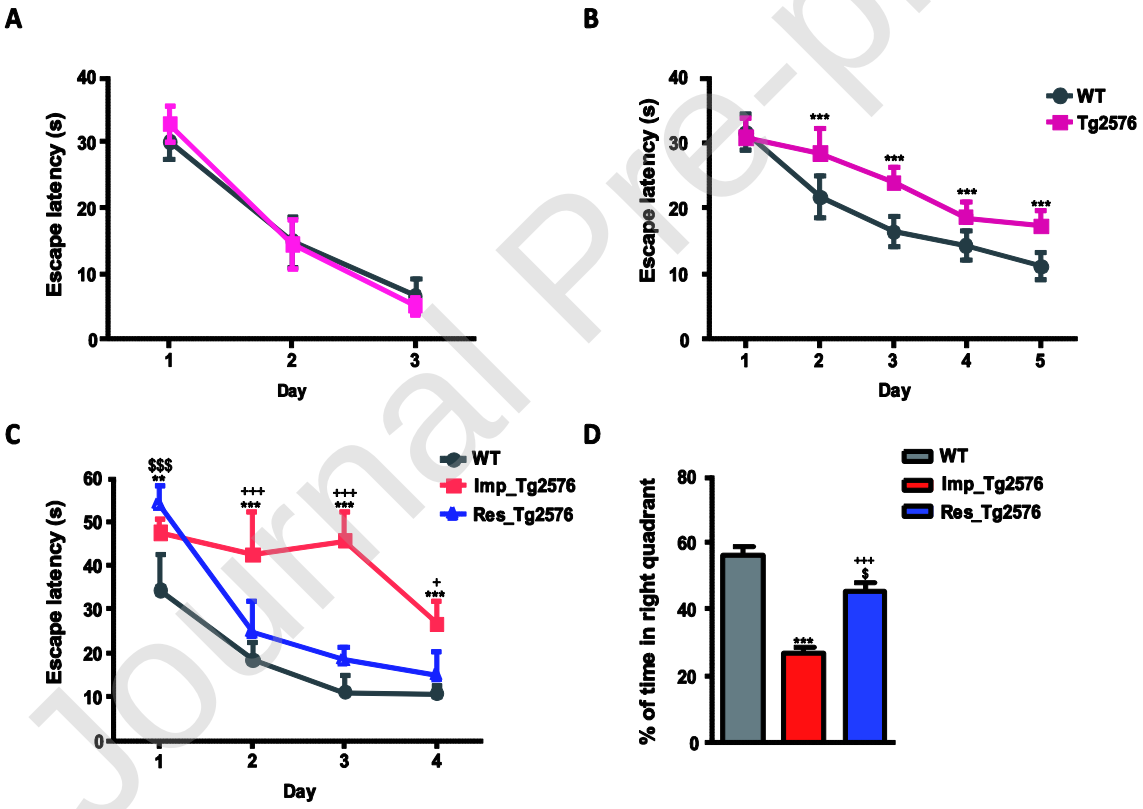

Figure 1

Figure 2

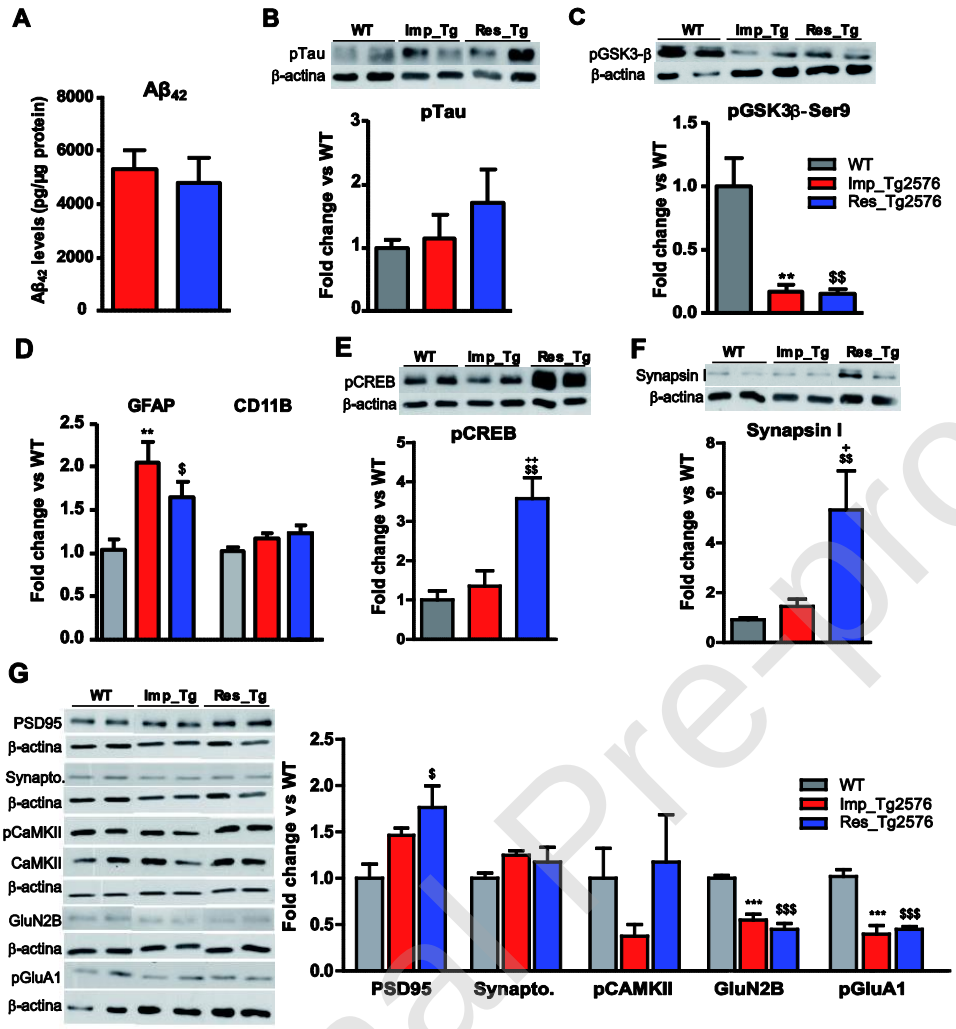

Figure 3

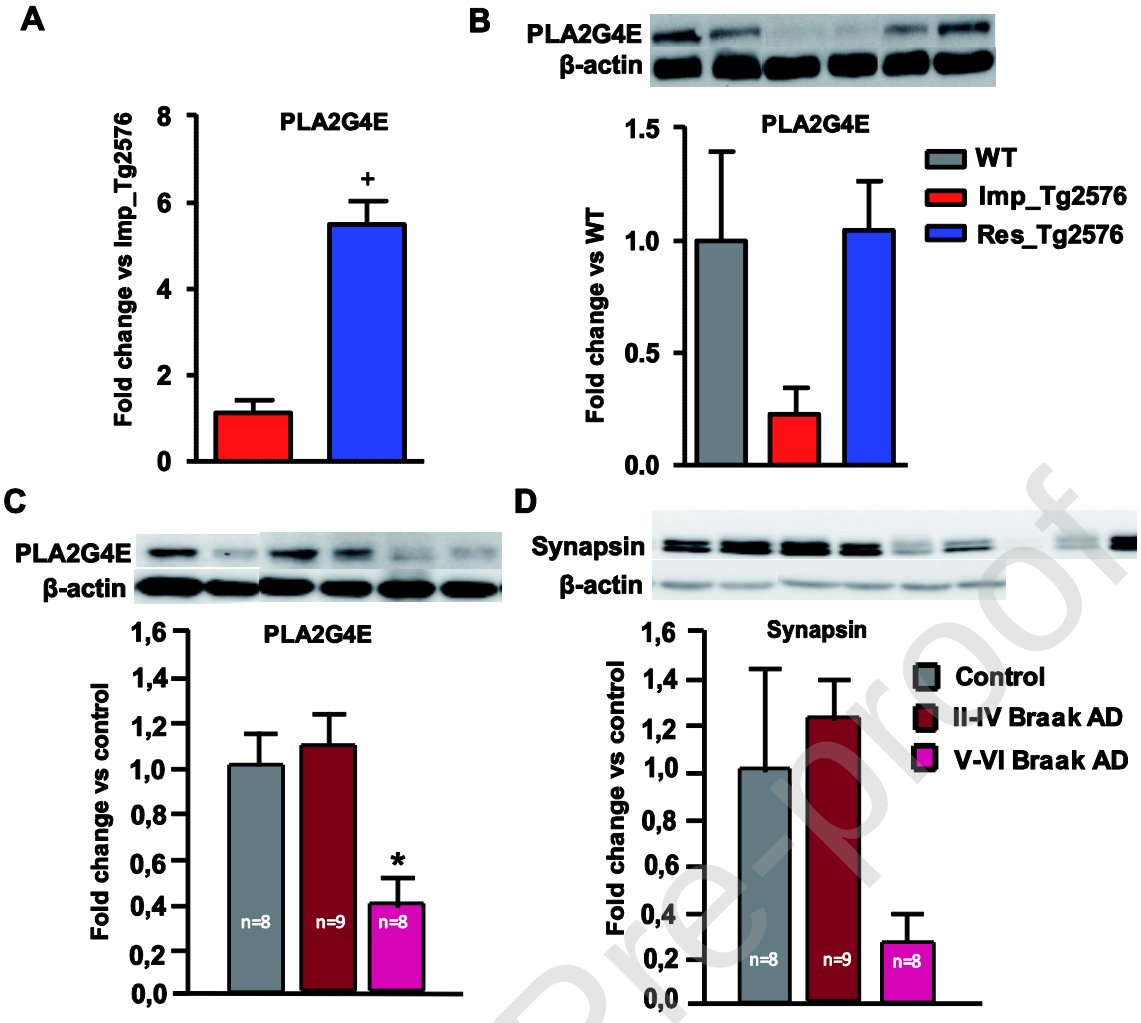

Figure 4

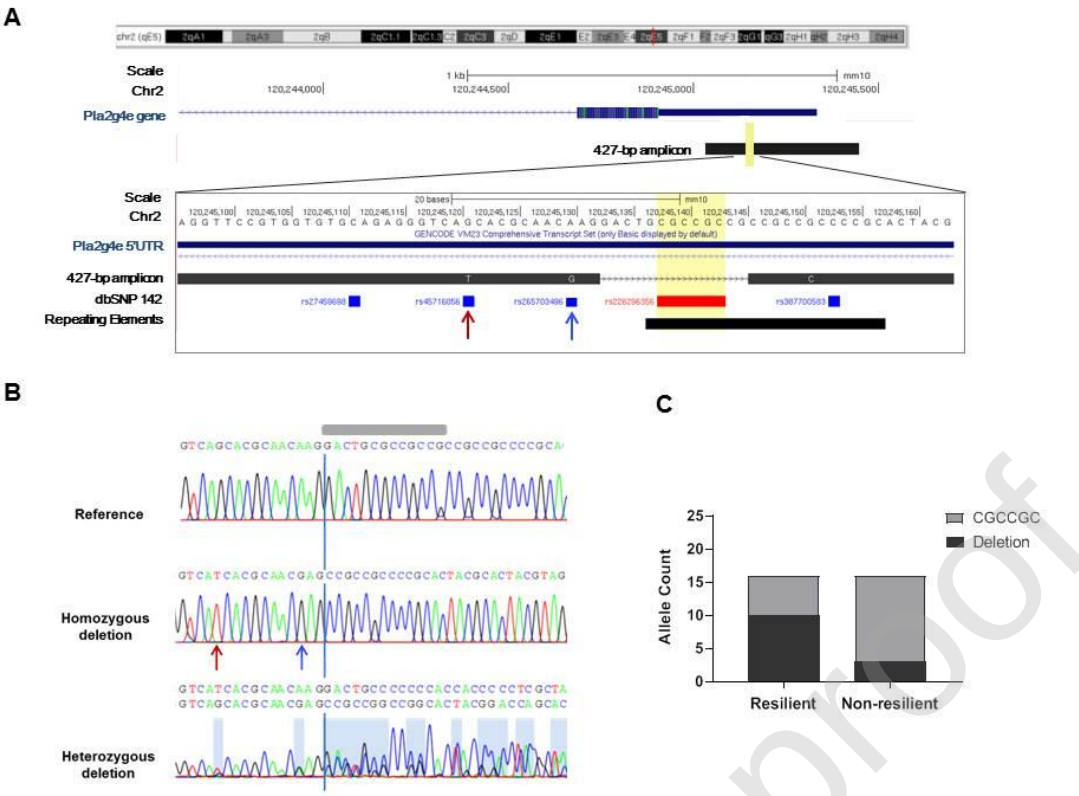

Figure 4

Figure 5

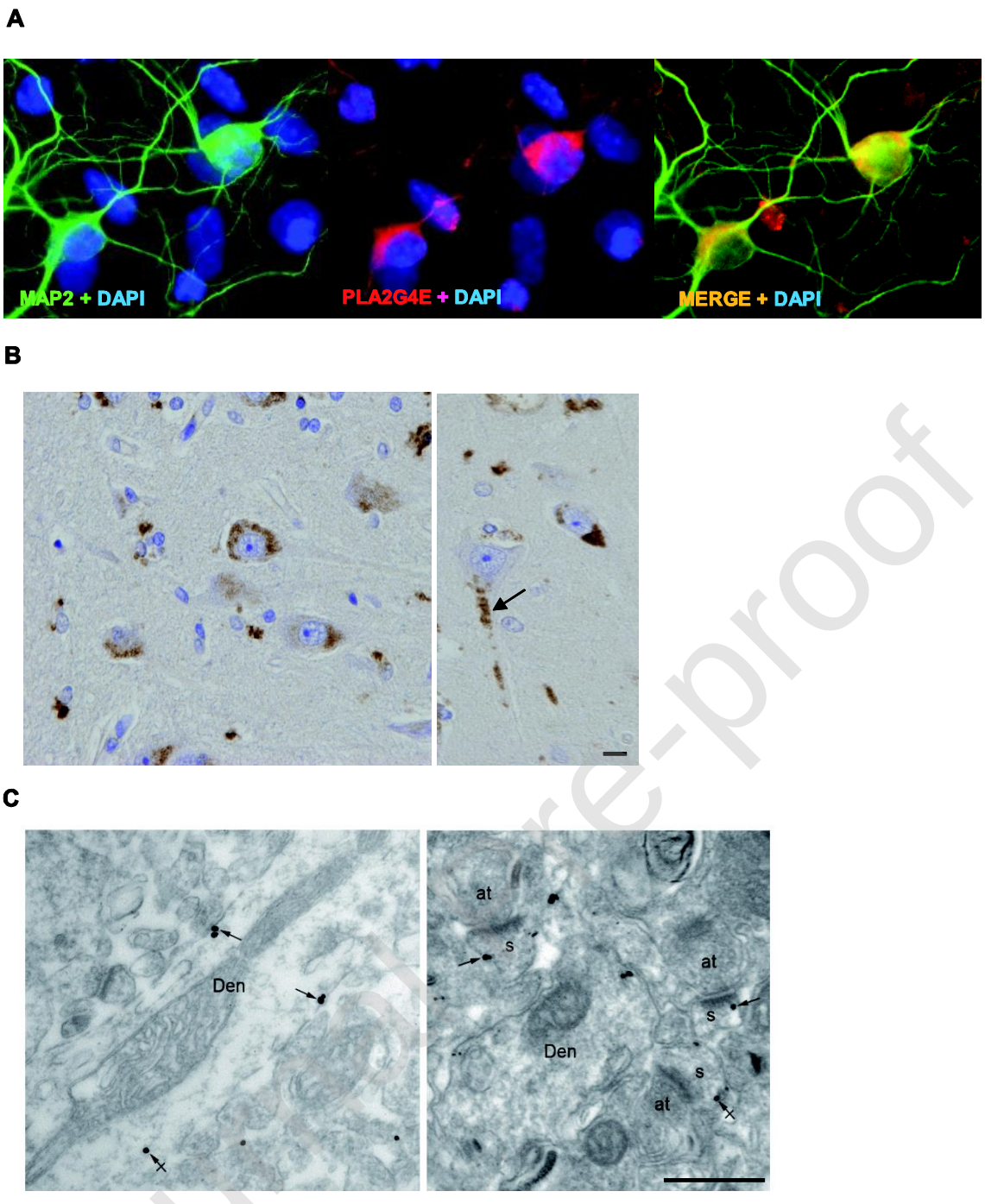

Figure 6

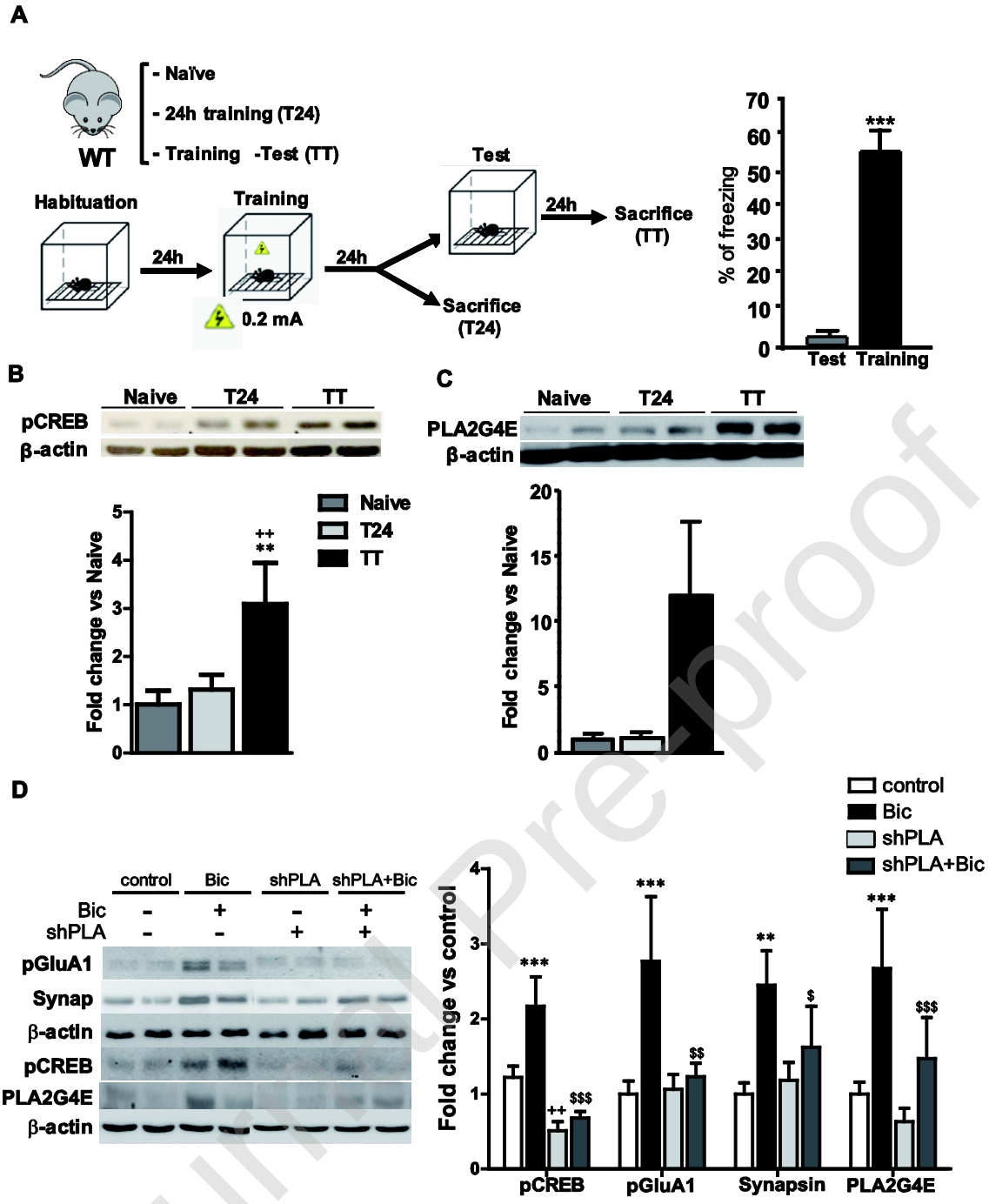

Figure 7